Atmos. Chem. Phys., 10, 8267–8286, 2010
www.atmos-chem-phys.net/10/8267/2010/
doi:10.5194/acp-10-8267-2010

Atmospheric Chemistry and Physics

Stratospheric water vapour budget and convection overshooting the tropopause: modelling study from SCOUT-AMMA

X. M. Liu[1], **E. D. Rivière**[1], **V. Marécal**[2], **G. Durry**[1], **A. Hamdouni**[1], **J. Arteta**[2,*], **and S. Khaykin**[3]

[1]Groupe de Spectrométrie moléculaire et Atmosphérique (GSMA), Université de Reims Champagne-Ardenne (URCA) and CNRS, UMR 689, Reims, France
[2]Laboratoire de Physique et Chimie de l'Environnement et de l'Espace (LPC2E), CNRS and Université d'Orléans, France
[3]Central Aerological Observatory of Roshydromet 3, Pervomayskaya str. Dolgoprudny, Moscow region 141700, Russian Federation, Russia
[*]now at: Centre National de Recherche Météorologique (CNRM), Météo-France and CNRS, Toulouse, France

Received: 9 December 2009 – Published in Atmos. Chem. Phys. Discuss.: 11 February 2010
Revised: 29 July 2010 – Accepted: 2 August 2010 – Published: 3 September 2010

Abstract. The aim of this paper is to study the impacts of overshooting convection at a local scale on the water distribution in the tropical UTLS. Overshooting convection is assumed to be one of the processes controlling the entry of water vapour mixing ratio in the stratosphere by injecting ice crystals above the tropopause which later sublimate and hydrate the lower stratosphere. For this purpose, we quantify the individual impact of two cases of overshooting convection in Africa observed during SCOUT-AMMA: the case of 4 August 2006 over Southern Chad which is likely to have influenced the water vapour measurements by micro-SDLA and FLASH-B from Niamey on 5 August, and the case of a mesoscale convective system over Aïr on 5 August 2006. We make use of high resolution (down to 1 km horizontally) nested grid simulations with the three-dimensional regional atmospheric model BRAMS (Brazilian Regional Atmospheric Modelling System). In both cases, BRAMS succeeds in simulating the main features of the convective activity, as well as overshooting convection, though the exact position and time of the overshoots indicated by MSG brightness temperature difference is not fully reproduced (typically 1° displacement in latitude compared with the overshoots indicated by brightness temperature difference from satellite observations for both cases, and several hours shift for the Aïr case on 5 August 2006). Total water budgets associated with these two events show a significant injection of ice particles above the tropopause with maximum values of about 3.7 ton s^{-1} for the Chad case (4 August) and 1.4 ton s^{-1} for the Aïr case (5 August), and a total upward cross tropopause transport of about 3300 ton h^{-1} for the Chad case and 2400 ton h^{-1} for the Aïr case in the third domain of simulation. The order of magnitude of these modelled fluxes is lower but comparable with similar studies in other tropical areas based on models. These two estimations exhibit significant differences and highlight variability among the cases of the impact of overshooting convection in hydrating the lower stratosphere. We show that the regional enhancement of water above the tropopause is between 0.21 to 0.67 ppmv between 380 and 400 K, generally in the range of other model estimations. The amount of water which remains in the stratosphere after the overshoot is estimated for both cases. A range of 330 to 507 tons is found for the Chad case and an upper limit of 200 tons is found for the Aïr case. Finally we emphasize that the hydrated area in the LS by overshooting convection can be advected relatively far away from the overshoot initial location, with locally mixing ratios of more than 3 ppmv higher than the background level, which is compatible with the balloon borne measurements performed above Niamey in the same air mass, 30 h after the overshoot.

Correspondence to: X. M. Liu
(xiaoman.liu@univ-reims.fr)

1 Introduction

Water vapour is a key component of the stratosphere, both for climate and chemistry. As the most important greenhouse gas in the atmosphere, the amount of water vapour in the stratosphere can significantly affect the earth's climate. It

also affects the ozone layer chemistry since water vapour is one of the main sources of OH hydroxyl radicals in the stratosphere and favours ozone depletion in winter by polar stratospheric cloud formation. A 1% increase of water vapour per year in the stratosphere was observed (Oltmans et al., 2000; Rosenlof et al., 2001) during the second half of the last century, which is believed to be partially due to water vapour transport across the tropical tropopause. This trend is still debated since Scherer et al. (2008) estimate a 0.7% increase but Randel et al. (2006), Jones et al. (2009) and Solomon et al. (2010) rather conclude a decrease after 2000. The understanding and the prediction of water vapour distribution in the tropical upper troposphere (UT) and lower stratosphere (LS) is currently a key issue since this region is likely to control the entry of water vapour in the stratosphere. At local scale, one important process controlling the water amount in the LS is overshooting convection, injecting directly ice crystals above the tropopause which later sublimate and hydrate the LS (Pommereau and Held, 2007).

Until recently, the most accepted mechanism driving the water vapour mixing ratio in the lower stratosphere is dehydration by freezing. This freezing is followed by sedimentation during the very slow ascent (6 months between 15 and 20 km) of tropospheric air due to positive radiative heating (Holton and Gettelman, 2001; Randel et al., 2001; Gettelman et al., 2002; Fueglistaler et al., 2004; Fueglistaler et al., 2005) in the Tropical Tropopause Layer (hereafter TTL, Fueglistaler et al., 2009). This is often referred to as the cold trap hypothesis. Concurrently, recent total water and water vapour measurements from aircraft and balloons show the presence of thin layers of enhanced water vapour or sometimes ice crystals up to several kilometres above the tropopause (Pommereau and Held, 2007; Nielsen et al., 2007; Chaboureau et al., 2007; Corti et al., 2008; Khaykin et al., 2009). They are attributed to convective overshoots and lead to the hydration of the lower stratosphere. As also seen by the TRMM Precipitation Radar and Lightning Imaging Sensor, these injections seem to occur mainly over land (Liu and Zipser, 2005; Zipser, 2006) even if the earlier study of Gettleman et al. (2002) concludes that the maximum occurs above the Pacific region. Although such events can be simulated by Cloud Resolving Models (Chaboureau et al., 2007; Grosvenor et al., 2007; Chemel et al., 2009) they have a too small horizontal size (10–20 km) and are of a too short duration (typically of one hour or less) to be captured by global Numerical Weather Prediction (NWP) models in which their representation cannot be taken into account explicitly. The existence of such events is now widely accepted but what is still unknown is their importance at the seasonal scale and at global scale, which depends of their frequency in a given convective area. Also unknown is their relative quantitative impact with respect to large-scale mechanisms such as the cold trap. Aiming at a deeper investigation of the mechanism of hydration of the lower stratosphere by convective overshoots, a series of simultaneous water vapour, particle and ozone measurements has been carried out within a SCOUT-AMMA (Stratosphere-Climate Links With Emphasis On The UTLS – African Monsoon Multidisciplinary Analysis) campaign in August 2006 from Niamey, Niger (13.6° N) in West Africa (Cairo et al., 2010). This is a location of frequent overshoots during the monsoon season according to Liu and Zipser (2005).

Although during SCOUT-AMMA the set of water measurements by several types of instruments onboard different platforms provides an unprecedented documentation of the UTLS tropical water vapour distribution, they are not sufficient to provide a full picture of the relative impact of the different processes affecting this distribution in the tropics. Conversely, a modelling approach, evaluated by such a set of measurements can be used to complement these observations and to quantify the impact of these processes. In particular three-dimensional limited-area meteorological models (mesoscale models) with fine resolution, down to that of cloud resolving simulations can solve explicitly deep convection, and are able to represent in a consistent manner dynamical and microphysical processes responsible for the water amount in the LS. Quantifying precisely the impact of single overshooting deep convection events on the LS hydration is a key step before those results can be extrapolated at a wider scale and before parameterizations of overshoots can be developed for global models. The relative impact of overshoots with respect to the freezing/drying mechanism in the TTL on the water budget could be then estimated. Recent studies (Schiller et al., 2009; James et al., 2008; Fueglistaler et al., 2005) conclude that the slow ascent leading to freezing/drying in the cold trap is predominant, with trajectory calculations roughly explaining the water distribution above the tropical tropopause. Nonetheless Schiller et al. (2009) also conclude that the impact of overshooting convection is still detectable at the local scale up to 420 K. Another important argument showing that the cold trap cannot explain alone the amount of water entering the tropical stratosphere concerns the trends of the tropical tropopause temperature: a decrease by 0.5 K decade^{-1} reported in Seidel et al. (2001) should lead to an enhancement of the dehydration at the tropopause, and thus to a decrease of the water amount in the stratosphere. This is not consistent with the observed trends of water vapour (Oltmans et al., 2000), suggesting that other mechanisms must play a significant role.

Only few estimations of the impact of single overshooting events are available in the literature and correspond to different areas of the globe - Maritime continent for Chemel et al. (2009), Brazil for Chaboureau et al. (2007) and Grosvenor et al. (2007) – and different models, leading sometimes to different impact at the local scale. The present work focuses on Africa, an area known for the relatively high frequency of overshoots according to Liu and Zipser (2005), and where no estimation of LS water injection by overshoot has been provided by CRMs up to now. Thus the aim of this study is to quantify the amount of water injected into the stratosphere

by two overshooting events in Africa: the first one is composed of several cloud clusters, and the second one is a well organised MCS. We also aim at complementing the few estimates already available in the literature which are necessary before parameterization of overshoots in global models can be developed.

The present work is based on the use of the three-dimensional regional and cloud resolving model BRAMS (Brazilian Regional Atmospheric Modelling System) (Freitas et al., 2009). It will be used to examine how a single overshooting deep convective system affects the water content of the TTL at the local scale in Africa. Here we study two overshooting cases observed in Niger and Chad during SCOUT-AMMA (Cairo et al., 2010), a European funded campaign part of the SCOUT-O3 programme, synchronous with the international AMMA project (Redelsperger et al., 2006): the case of 4 August 2006 over Southern Chad that likely influenced the water vapour balloon-borne measurements of 5 August in Niamey (Khaykin et al., 2009, hereafter K2009), and the case of 5 to 6 August 2006 of a mesocale convective system (MCS) generated over central Niger which later propagated toward Niamey and Burkina Faso.

The paper is organized as follows. Section 2 gives an overview of the convective events. Section 3 describes the numerical tool used in this study as well as the experimental data. Section 4 discusses the ability of the model to simulate the observed cases. Section 5 is dedicated to the calculation of water transport to the lower stratosphere by overshooting convection and its impact at local/regional scale in the LS. The conclusions are given in Sect. 6.

2 Overview of the observation of the convective event

Two cases of overshooting convection are presented in this paper. Both of them occurred in a relatively active period. The first one took place over Southern Chad on 4 August 2006 and is referred hereafter as the "Chad case". The second case occurred in Aïr (central Niger) on 5 August 2006. In the following, it will be referred as the "Aïr case".

2.1 Description of the Chad case

Balloon borne water vapour measurements on 5 August 2006 from the Niamey military airport (13°29′ N, 02°19′ E) by micro-SDLA onboard the "water vapour flight no. 1" launched at 18:40 UT and by FLASH-B launched at 18:52 UT are shown in Fig. 1. Micro-SDLA is a tunable diode laser spectrometer devoted to the in situ measurement of H_2O, CH_4 and CO_2 by infrared absorption spectroscopy (Durry et al., 2004). Three near-infrared telecommunication-type InGaAs laser diodes are connected by means of optical fibres to an open multi-path optical cell providing an absorption path-length of 28 m. The laser beam is absorbed by ambient gas molecules as it is bouncing back and forth between the cell mirrors. H_2O is monitored at 1.39 µm using the differential detection technique. The payload also includes pressure and temperature sensors. The accuracy of the H_2O measurements within 160 ms is 5%. Micro-SDLA was already flown successfully in the tropics during the HIBISCUS campaign (Marécal et al., 2007). FLASH is a Lyman-α hygrometer. The instrument as well as its measurements performed on 5 August 2006, 12 min later than micro-SDLA is described in K2009. Although the fine structures of the micro-SDLA profile shown in Fig. 1 are qualitatively consistent with FLASH observations on the same day, micro-SDLA shows a still unexplained dry bias. We suspect this bias could be due to a mis-adjustment of the optical multi-pass cell so that a wrong value for absorption path length was used in the concentration retrieval process for the water vapour channel.

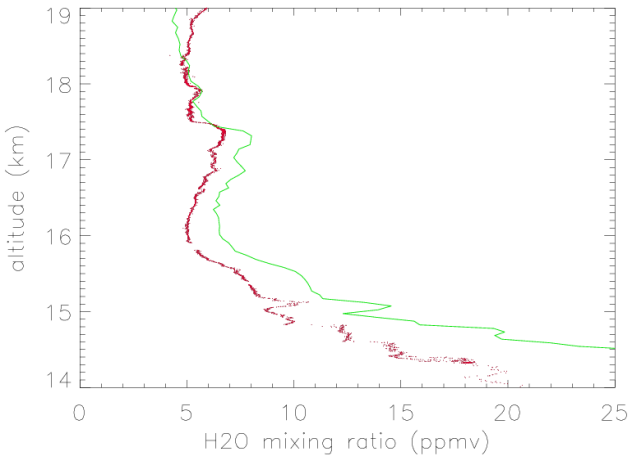

Fig. 1. UTLS water vapour profiles from Balloon-borne micro-SDLA (red line) and FLASH-B (green) measurements from Niamey at 18:40 and 18:52 UT (launch time) on 5 August 2006, respectively.

The study of this case was motivated by a layer of enhanced water vapour around 17–17.5 km altitude, seen by both instruments in Fig. 1. The enhancement of water vapour with respect to the background value in this layer is about 2 ppbv for both instruments, and the corresponding mixing ratios are 8 ppmv for FLASH and 7 ppmv for micro-SDLA. This layer is located significantly above the tropopause (∼16.5 km). Using backward trajectories based on ECMWF operational analysis winds, K2009 have related this enhancement to overshooting convection from deep convection over Southern Chad on 4 August 2006, 14:30 UT.

Figure 2 shows a series of Meteosat Second Generation (MSG) IR images in the 10° E to 30° E and 0° N to 20° N domain describing the time evolution of the convective activity in the Sudan/Chad area for this "Chad case". The convective activity begins at 10:30 UT on the Sudan-Chad border. It develops further in a cluster of several cloud

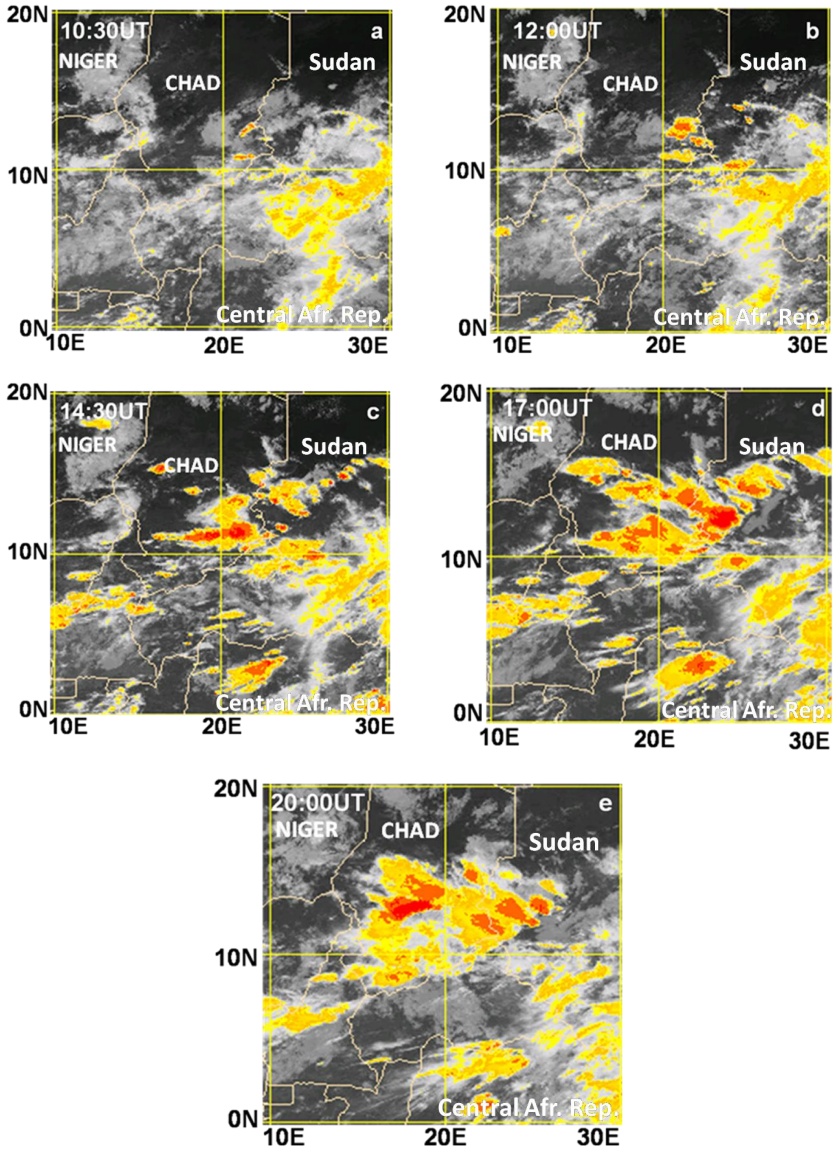

Fig. 2. Meteosat Second Generation Infrared images in the 10° E to 30° E longitude range and in the 0° N to 20° N latitude range on 4 August 2006 at **(a)** 10:30 UT **(b)** 12:00 UT **(c)** 14:30 UT **(d)** 17:00 UT **(e)** 20:00 UT.

systems, South-East of Chad at 12:00 UT (Fig. 2b). At ∼12:14 UT, the Lidar instrument CALIOP onboard the Cloud-Aerosol Lidar and Infrared Pathfinder Satellite Observation (CALIPSO) satellite scanned the convective cloud cluster (not shown). The CALIPSO measurements highlight that the cloud top of the cloud cluster is typically at 16.5 km in the latitude range 10° N to 13° N and that some parts of this cloud top are classified as "stratospheric features" in the version 2.0.1 of the feature mask products. Although the class "stratospheric features" is not always unambiguous (see CALIPSO Quality Statement Lidar level 2 vertical feature mask at http://eosweb.larc.nasa.gov/PRODOCS/calipso/Quality_Summaries/CALIOP_L2VFMProducts_2.01.html), CALIOP measurements confirm that at about 12:12 UT the cloud top is very close to the tropopause. At 14:30 UT (Fig. 2c), the convective area is composed of an East-West band of clouds (from 22° E to 16° E; ∼11° N). North-East of this band, there is another cloud system area that joins the first one while it is decaying. East of the Chad/Sudan border, cluster of several convective clouds are growing. This is the time when K2009 identify overshooting convection from the 11° N East-West band of cloud from brightness temperatures analysis. They identified from a trajectory analysis that the LS air coming from the overshoot moved toward the Niamey area and was sampled by the FLASH-B instrument above Niamey (Fig. 1). At 17:00 UT (Fig. 2d), the 11° N East-West

band spreads South and North while convective activity develops on the Eastern to North-Western part of it. At 20:00 UT (Fig. 2e) the convective activity is mainly around 17° E, 12.5° N, coming both from the North-East and from the former 11° N band that join together.

To identify the location and time of the overshoots associated with the convective activity in the Southern Chad area we use a detection method of overshoots from Meteosat Second Generation (MSG) observations. This method (Schmetz et al., 1997) is based on the brightness temperature difference (hereafter BTD) between the 6.2 µm and the 10.8 µm channel. The first channel is sensitive to the water vapour emission in the warmer temperature of the lower stratosphere with respect to the adiabatically cooled overshooting turret temperature. The BTD threshold for the detection of overshoot is set to 3 K as in Chaboureau et al. (2007) and K2009. In a study of deep convection over the Indian Ocean, Roca et al. (2002) use a larger BTD threshold of 5 K. However, it has been checked for a specific overshoot observational case of SCOUT-AMMA in the afternoon of 23 August 2006, that the MSG BTD was about 3.2 K while the MIT radar at Niamey sampled a convective cell reaching 18.3 km well above the tropopause (∼16.5 km). This proves that the threshold of BTD=3 K for the detection of overshoot is realistic in this region of Africa. Figure 3 shows the MSG pixels with BTDs higher than 3 K for the 12:15 UT to 19:15 UT with a 15-min time resolution. It shows that the overshooting convection activity mainly occurs in the 11° N East-West band of clouds, and moves with time Westward. 14:30 UT is the time when K2009 identify 23 overshooting pixels in this area, to be of the same air mass as the one sampled by FLASH 30 h later above Niamey. From 15:45 UT, overshooting pixels appear North of this band (typically 12° N, 20.5° E). From 17:00 UT, an area of overshoot is given by MSG observations in West Sudan (12° N, 23° E) and corresponds to a large red area in Fig. 2d. From 19:00 UT, another area of overshooting pixels appears around 12.3° N 17.8° E. It corresponds to the high convective activity shown in Fig. 2e coming both from the spreading of the former East-West cloud band and the Northern cloud cluster.

To summarize, the period after 12:00 UT on 4 August 2006 in Southern Chad is a period of severe deep convection including overshoots in several subareas: the 11° N East-West band of clouds at 14:30 UT, the area in Sudan close to the Chad border at 17:00 UT, and later the North-West area at 20:00 UT. Satellite images (Fig. 2) show that the different cloud bands interact with each other to create a large cloud cluster.

2.2 Description of the Aïr case

A mesoscale convective system was observed East/North-East of Niamey at the time of the balloon-borne measurements on 5 August 2006. Figure 4 shows the time evolution of this "Aïr case" MCS as seen by MSG. Convection triggers

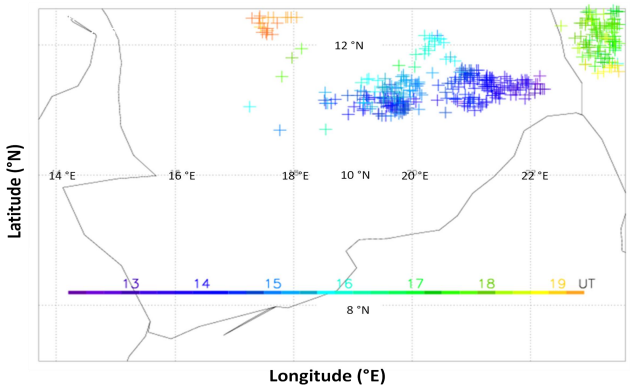

Fig. 3. MSG pixels with brightness temperature difference (BTD) higher than 3 K between the 6.2 µm channel and the 10.8 µm channel in Southern Chad from 12:30 UT to 19:30 UT on 4 August 2006. The time resolution of MSG data is 15 min.

in the Aïr mountain area (centre Niger) at about 13:30 UT (Fig. 4a) in the 8.5° E, 17° N to 19° N area. Another active cloud area is observed close to the Niger/Nigeria/Chad border. The Aïr system grows and extends to 15° N and 7° E on 5 August (Fig. 4b) becoming an organized Mesoscale Convective System (MCS) at 18:00 UT. At the same time, the Niger/Nigeria cloud system grows and propagates westward. The Aïr MCS grows and moves westward until 18:00 UT (Fig. 4c) when it reaches its top activity. At the same time the Niger/Nigeria/Chad cloud cluster has decayed and split into two different parts: the first one stays at the Chad Niger border while the second, at the Niger/Nigerian border (10° E), continue to propagate westward. It later joins the Aïr MCS while the latter propagates south-westward towards Niamey (Fig. 4d). The total system reaches Niamey in the morning of 6 August and will later move to Burkina Faso while decaying.

Using the same MSG brightness temperature difference technique as for the "Chad case", we have checked the occurrence of overshooting activity of the Aïr MCS. Figure 5 shows the overshooting pixels in central Niger for the period from 14:45 UT to 17:30 UT. It shows that the Aïr area has experienced overshooting convection during this period. The overshooting area moves westward (slightly northward) with time, which is compatible with the westward propagation of the MCS during its maximum of activity. At 15:30 UT, 16:15 and 16:30 UT the number of pixels with BTD>3 K is 13, 14, and 16, respectively. These numbers are smaller than for the Chad case: at 14:30 UT, K2009 have reported a total of 23 pixels with BTD>3 K (see Table 2 of K2009 for details about the Chad Case BTDs). Table 1 summarizes the time evolution of the overshoot size in pixels. It shows that the most intense overshooting activity is between 15:30 UT and 16:30 UT with a maximum BTD of 4.8 K which is close to the overshoot criteria proposed by Roca et al. (2002).

Table 1. Time evolution of the overshoot size in MSG pixels for the Aïr case, from 14:45 UT to 17:30 UT. At each time, the maximum BTD is also reported. BTD: Brightness Temperature Difference between the 6.2 µm and the 10.8 µm channels.

Time of overshoot (UT)	Size of overshoot (number of pixels)	Maximum BTD value of the overshoot
5 August 14:45	3	3.49
5 August 15:00	3	3.06
5 August 15:15	3	3.27
5 August 15:30	13	4.8
5 August 15:45	5	3.87
5 August 16:00	8	3.52
5 August 16:15	14	3.87
5 August 16:30	16	3.89
5 August 16:45	11	3.87
5 August 17:00	6	3.59
5 August 17:15	3	3.79
5 August 17:30	2	3.92

In the following we study both the Chad case and the Aïr case with a mesoscale model. It will give an opportunity to compare the impact of different types of system on the lower stratosphere hydration by overshooting convection. The next section describes the modelling tools and model setup used in this study.

3 Modelling tools and simulation setup

The Brazilian Regional Atmospheric Modelling System (BRAMS) model is a mesoscale model tailored to the tropics. It is the Brazilian version of the RAMS model (Cotton et al., 2003) of the University of Colorado/ATMET. BRAMS (Freitas et al., 2009) was developed at CPTEC (http://brams.cptec.inpe.br/). It is designed to simulate atmospheric circulations at different scales from large regional simulations down to large eddy simulations. It includes a full set of parameterizations for surface processes, radiative scheme, dynamics, sub grid scale convection and microphysics. BRAMS differs from RAMS in improvements concerning cumulus convection parameterization, soil moisture initialization and surface scheme. BRAMS/RAMS offer the possibility to use nested grids, each grid communicating in a two way process with its parent or child grid. BRAMS was successfully used to simulate water vapour distribution in the tropical UTLS in a deep convective environment over Brazil (Marécal et al., 2007).

Two simulations were run using the BRAMS model for each of the case studies described in Sect. 2. For both simulations, the radiative scheme of Harrington (1997) was used for short and long wavelengths. The sub grid scale parameterization of shallow and deep convection of Grell and Devenyi (2002) was chosen. The setup for microphysics makes use of the two moment scheme developed by Meyers et al. (1997). Seven types of hydrometeors are taken into account in the model: liquid cloud droplets and rain for liquid particles, and pristine, snow, hail, graupel and aggregates for ice particles. In this scheme, both hydrometeor number concentrations and mass mixing ratios are prognostic variables of the model, assuming that each hydrometeor size distributions follows a gamma function. In the simulation the shape parameter of the gamma function is assumed to be 2 for each category of hydrometeors as successfully used with BRAMS in Pénide et al. (2010) for AMMA case simulations. Although considered as a bulk scheme, this relatively detailed scheme is particularly suitable for the quantification of water transport across the tropopause by overshooting convection, in which ice particles are supposed to play an important role (Pommereau and Held, 2007; Grosvenor et al., 2007; Chemel et al., 2009): as a matter of fact, the number of hydrometeors is higher than for other CRMs already used for studying the role of overshooting convection on the LS hydration. The Meso-NH model used in Chaboureau et al. (2007) and the ARW model used in Chemel et al. (2009) have 5 types of hydrometeors (including 3 classes of ice particles). Furthermore double moment schemes used in BRAMS and ARW are said to be more precise than single moment schemes as in Meso-NH. These differences among models are likely to induce differences in the simulated amount of water injected by overshooting convection.

Table 2. Model setting used for the Chad (4 August 2006) and Aïr (5 August 2006) case simulations. Size, resolution and starting time for each grid are reported.

Cases	Grid setting			
	Grid	Horizontal resolution (km)	Grid points (NX, NY, NZ)	Model start (UT)
Chad	G1	20 × 20	93, 83, 68	3 August, 18:00
	G2	4 × 4	242, 157, 68	
	G3	1× 1	214, 110, 68	
Aïr	G1	20 × 20	152, 154, 68	5 August, 00:00
	G2	4 × 4	162, 197, 68	
	G3	1 × 1	106, 118, 68	

Global ECMWF (European Centre for Medium-range Weather Forecasts) 6-hourly analyses were used in this study, both for the initialization and the nudging at the lateral boundaries of the larger BRAMS domain (Grid 1). The set of analyses used are the special AMMA reanalyses done at ECMWF (Agusti-Panareda et al., 2009, 2010), which take into account all the radio sonde measurements of the AMMA campaign in West Africa. Sensitivity tests have been performed using operational analyses instead of AMMA reanalyses and showed a significant improvement of the BRAMS results using the reanalyses in term of convective system formation, severity, lifetime and propagation.

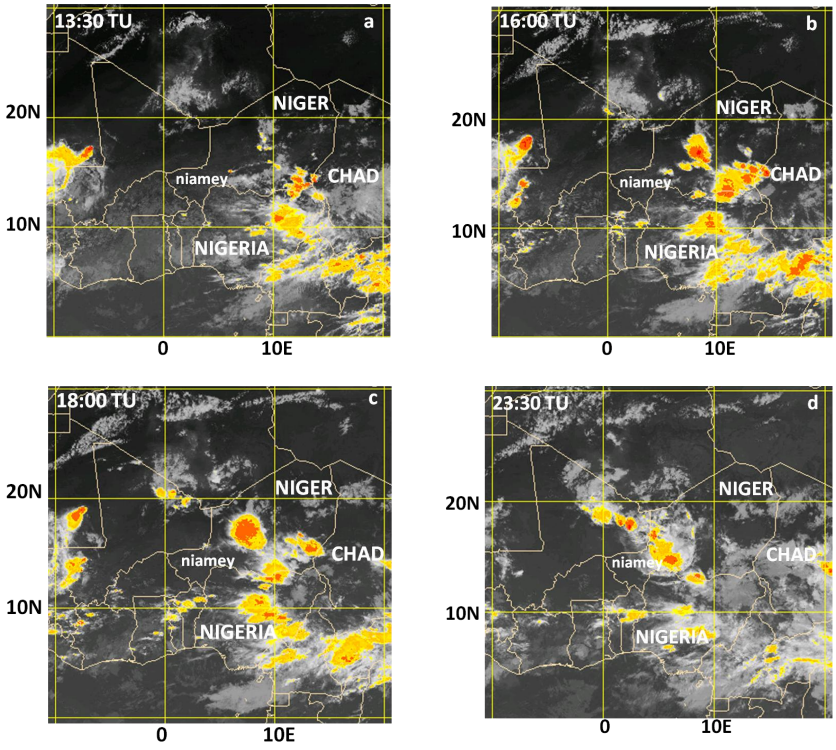

Fig. 4. MSG Infrared images centered on Niger on 5 August 2006. **(a)** 13:30 UT **(b)** 16:00 UT **(c)** 18:00 UT **(d)** 23:30 UT.

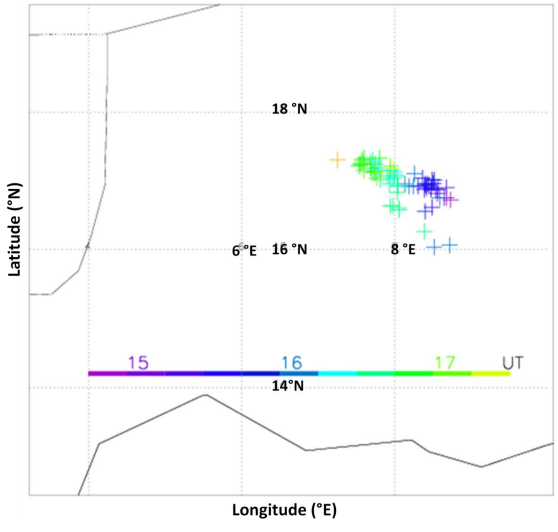

Fig. 5. Same as Fig. 3 but for the Aïr case from 14:45 UT to 17:30 UT on 5 August 2006.

3.1 Specific setting for the Chad case

The 4 August 2006 convective system simulation includes three nested grids as shown in Fig. 6a. The coarse grid (Grid 1) covers a domain from ∼8.20° E to 25.94° E in longitude and from 2.39° N to 17.78° N in latitude including the Atlantic Ocean in the South-West corner. Its horizontal grid spacing is 20 km. A finer resolution second grid (Grid 2), including the area where most of the deep convection was observed, extends from 15.18° E to 24.28° E in longitude and from 8.88° N to 14.68° N in latitude with 4 km grid spacing. The finest grid has 1 km grid spacing and covers a 214×110 km domain from 19.98° E to 21.93° E in longitude and from 11.15° N to 12.19° N in latitude focused in the area of the East-West cloud band in its mature phase in order to properly take into account the overshoot area highlighted by K2009. The topography is also reported in Fig. 6, indicating within Grid 3 a region with hills higher that 800 m, and within Grid 2 an area in Sudan with topography higher than 1300 m. For all these grids, the vertical coordinate is terrain-following height coordinate with 68 levels from the surface to 30 km altitude with 300 m spacing in the UTLS. In order to damp the gravity waves at the top of the domain, an absorbing layer of 5 km thickness was prescribed at the top boundary. The time steps used are 30 s, 10 s and 2 s for Grid 1, Grid 2 and Grid 3, respectively. The simulation was initialized at 18:00 UT on 3 August 2006 and ended on 5 August at 12:00 UT. Model outputs were saved every hour except during the most intense period of convection in the model from 4 August, 12:00 UT to 20:00 UT when model outputs were saved every five minutes. The choice of the model configuration was a trade-off between high resolution and computing cost.

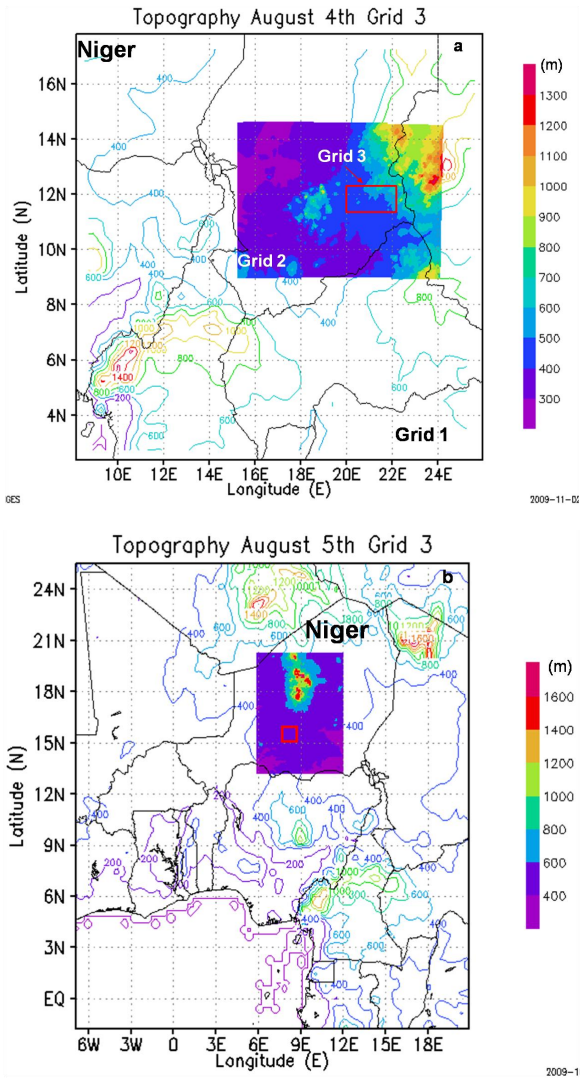

Fig. 6. Topography of the 3 nested grids used for the BRAMS simulation (iso-lines for Grid 1, and shaded contour for grids 2 and 3). **(a)** Chad case. **(b)** Aïr case.

3.2 Specific setup for the Aïr case

The Aïr system was also simulated with three nested grids (Fig. 6b). Grid 1 covers a domain from 7.942° W to 22.05° E in longitude and from 2.02° S to 26.10° N in latitude with 20 km grid spacing. This includes a large fraction of West Africa. A significant part of Grid 1 includes the Atlantic Ocean in order to better account for the monsoon flux. The domain of Grid 2 is from 5.80° E to 12.14° E in longitude and from 13.16° N to 20.36° N in latitude. This grid, with a relatively fine horizontal resolution (4 km grid spacing) covers the Aïr Mountains with height higher than 1600 m in the central Niger where the MCS of interest developed, as shown by the topography in Fig. 6b. Grid 3 has 1 km grid spacing and covers a 106 km by 118 km domain from 7.84° E to 8.83° E in longitude and from 15.36° S to 16.45° N in latitude, is located South of the Aïr Mountains. The location of Grid 3 is chosen in the area where the modelled convection is the most severe from a previous simulation with two grids only. The vertical coordinate and the time steps are the same as in the Chad simulation. The simulation was initialized at 00:00 UT on 5 August 2006 and was run for 24 h saving model outputs every hour except during the period 18:00 UT to 00:00 UT when model outputs were saved every 5 min to follow the detailed evolution of the overshoots.

4 Evaluation of the simulations

In this section, we evaluate the results of the two simulations against observations. We focus on the ability of the model to reproduce the observed deep convective systems/clusters at the regional scale in which the overshoots are embedded and also the observed overshoots locally. We compare BRAMS outputs with TRMM (Tropical Rainfall Measuring Mission) estimates of surface rainrates. The TRMM dataset used was produced by the 3B42 algorithm (Huffman et al., 2007, http://trmm.gsfc.nasa.gov). It is 3-hourly and $0.25° \times 0.25°$ resolution. The comparison is done using the Grid 1 results which include the mesoscale convective systems affecting the overshoot area. Moreover Grid 1 resolution is close to TRMM products (20 km for Grid 1 and 0.25° for TRMM). We also compare the model results to the MSG overshoot observations. This is done using the simulation fields from the finest resolution grid (Grid 3 with 1 km horizontal resolution). Overshooting convection can only be simulated when convective dynamical fields are explicitly resolved in the model, i.e. using a resolution $\leq$1 km, as shown in previous studies (Grosvenor et al., 2007; Chaboureau et al., 2007). Note that the observed overshoots are far from the AMMA/SCOUT-AMMA campaign zone. Therefore it was not possible to make comparisons with balloon borne or aircraft measurements close to the overshoots.

4.1 Chad case

Figure 7 shows comparisons of surface rainrates (expressed in mm h^{-1}) between TRMM (Fig. 7a, c, e) and BRAMS model outputs (Fig. 7b, d, f) for 15:00 UT (between 13:30 UT and 16:30 UT), 18:00 UT (between 16:30 UT and 19:30 UT), and for 21:00 UT (between 19:30 UT and 22:30 UT). Rainrates are accumulated over three hour periods. The focus being on the observed overshoots, we have displayed the model and observed surface rainrates over the sub-domain of Grid 1 including the convective systems that are likely to affect the overshoots. Note that this sub-domain is larger than Grid 2 area and includes the whole Grid 2 domain. During the period of interest, several convective systems develop and interact while advected as illustrated by the time evolution of the many features appearing in the TRMM surface precipitation

fields (Fig. 7a, c, f) and already discussed for MSG observations (see Sect. 2). The features of interest have been identified in Fig. 7a, c, e by blue and green colour contours.

The first one is highlighted by the green ellipse corresponding to an area of precipitation in the North-East of the domain close to the Sudan-Chad border. This rainband hardly moves between 13:30 UT to 22:30 UT. Only the intensity of the individual convective cells varies with time. BRAMS fairly well simulates the position of this rain area (Fig. 7b). However, BRAMS overestimates the intensity of this rain area with maxima over 10 mm h^{-1} while the maxima from TRMM are usually between 5 and 10 mm h^{-1}.

The second important precipitation feature is highlighted by a blue domain. At 15:00 UT both BRAMS and TRMM show an East-West band of precipitation at ∼11–11.5° N with the same intensity and distribution. This area corresponds to the zone where the K2009 Chad overshoot has been highlighted. It corresponds to the purple to blue overshooting pixel zone in Fig. 3. South of this band, BRAMS simulates a local maximum of the same intensity as the TRMM estimation. BRAMS only fails in the North of the domain where an isolated low precipitating cell seen by TRMM is simulated by BRAMS much further West in a larger area. Later at 18:00 UT (Fig. 7c) the TRMM products show that the precipitation zone spread North and South (Fig. 7c). This is also well captured by BRAMS (Fig. 7d), both in location and intensity. The Northern cell in the West of the domain given in TRMM products intensify, as well as the cell located more West in the BRAMS simulation which is at the West edge of the Grid 2 domain. At 21:00 UT the area of precipitation in the centre of the domain at 11° N 19° E for TRMM and 11.5° N 20° E for BRAMS is decaying. Concurrently, further West, for both TRMM and BRAMS, there is an intensification of the precipitation from North to South. A very intense area in the North-West is seen by TRMM (Fig. 7e) and corresponds to the orange overshooting pixels in Fig. 3. A detailed analysis of the MSG infrared images shows that this area is initially formed from an interaction between the Northern precipitating cells and the 11° N precipitating band. In the BRAMS simulation (Fig. 7f), intensification of the precipitation in the West from North to South is also visible, though the location is too far West.

To evaluate the overshooting activity in BRAMS with respect to the MSG BTD observations, Fig. 8 shows the Grid 3 points for which there is a significant ice amount (mass mixing ratio above 0.05 g kg^{-1}) above the tropopause, considered here as the 380 K level (Holton et al., 1995), during the time of overshoots in BRAMS. Dependence with time is indicated by the colour scale, chosen the same as in Fig. 3. Note that the horizontal resolution of the model in Grid 3 (1 km) is higher than the MSG resolution (∼3.3 km). It shows that the overshooting activity begins at ∼13:15 UT and ends at 14:45 UT. Except for a few overshooting points at 11.6° N from ∼13:15 UT, most of them are along the 12° N latitude and move with time from East to West (from 13:15 to 14:15 UT). This tendency both in time and location is in good agreement with the BTD overshooting pixels shown in Fig. 3, though the observed overshooting pixels are located along the 11.1° N latitude. This good agreement of the model with observations must be balanced by the fact that ice which is calculated to be produced in overshoots at 14:00 UT is advected westward in the LS before it sublimates totally. Thus the grid points with ice mixing ratio higher than 0.05 g kg^{-1} should not all be considered as overshot grid points but as grid points with ice of overshooting origin. On the other hand, it is possible that the BTD signature is also sensitive to advection of sublimating ice injected by overshoot when the cloud system below remains very active. Due to the limited size of the Grid 3 domain to save computing resources, the overall overshooting activity observed by MSG in all the Southern part of Chad cannot fully be reproduced by BRAMS. We chose to restrict our goal to reproduce the overshoots occurring in the time range and the location pointed out by K2009, shown to influence the FLASH-B/µ-SDLA measurements.

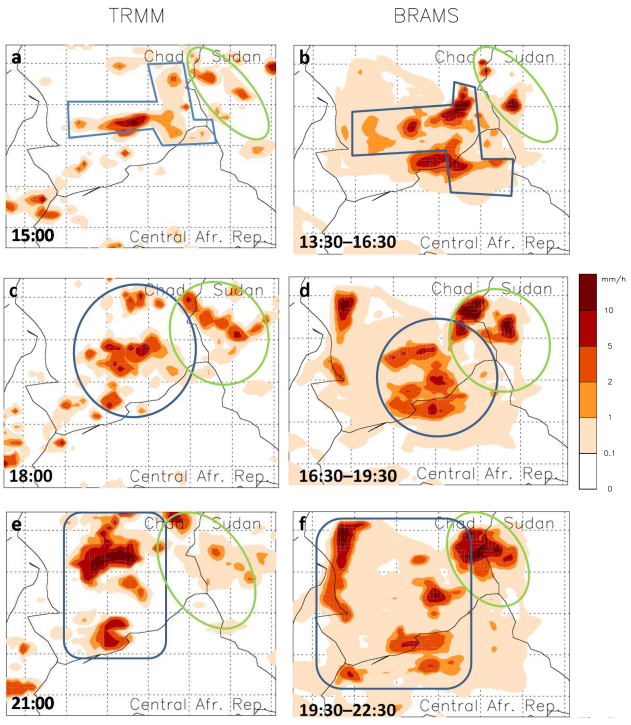

Fig. 7. Comparison between TRMM (**a, c, e**) and BRAMS (**b, d, f**) surface rainrate accumulated over 3 h periods for the Chad case. Panel (a) and (b): from 13:30 UT to 16:30 UT on 4 August 2006. Panel (c) and (d) from 16:30 to 19:30 UT. Panel (e) and (f) from 19:30 UT to 21:30 UT.

Figure 9 shows a vertical cross section of total water along the 12° N latitude in the BRAMS Grid 3 domain at 14:15 UT. It highlights that the simulated cloud system overshoots the tropopause up to 17.8 km, above the 400 K level. Note that the position and the time of this overshooting plume is in very good agreement with the overshoot highlighted by K2009.

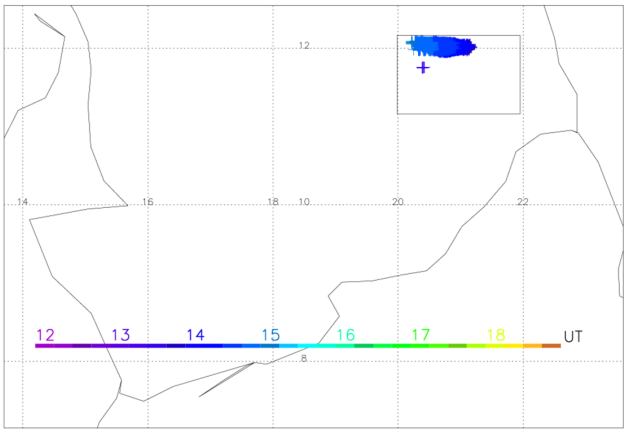

Fig. 8. Chad case BRAMS simulation. Grid 3 time evolution of the grid points having an ice mixing ratio higher than 0.05 g kg^{-1} above the tropopause (380 K). The same color scale as in Fig. 3 is chosen.

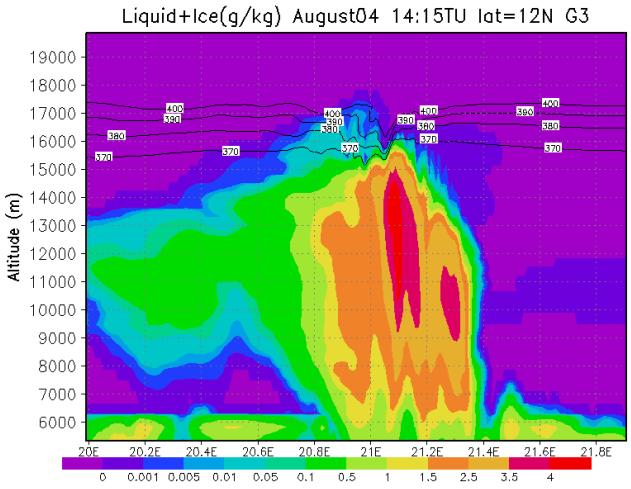

Fig. 9. Longitude/Altitude cross-section of condensed water mixing ratio (g kg^{-1}) around the overshoot location inside Grid 3 at 12° N latitude and 14:15 UT on 4 August 2006. The solid lines indicate the isentropic levels 370, 380, 390 and 400 K.

We have also computed the ice water content (IWC) in the grid 3 domain from 14:00 UT to 16:00 UT, and have compared them to measurements of stratospheric ice during previous campaigns in other continents, provided in Fig. 1 of Corti et al. (2008). This comparison shows that the IWC are comparable in both cases, confirming that our simulation is realistic, as discussed in more detail in Sect. 5.1.

To summarize, BRAMS succeeds in reproducing the main features of the observed precipitation, except in the West part of the domain from 18:00 UT where BRAMS produces precipitation which is seen by the satellite much further Est. The model provides good results in the center of the domain for the East-West band of precipitation where the K2009 overshoots are highlighted. The overshooting activity in the time range from 12:00 UT to 15:00 UT is in good agreement with the observations, and the ice content in the stratosphere is of the same order of magnitude as the ice sampled during previous airborne campaigns in other regions of the globe.

4.2 Aïr case

As for the Chad case we evaluate the simulation of the Aïr MCS on 5 August 2006 by comparing model outputs to TRMM rainrates and to BTD from MSG. Figure 10 shows comparisons of surface rainrates (expressed in mm h^{-1}) between TRMM (Fig. 10a, c, e) at 15:00 UT, 18:00 UT and 21:00 UT, respectively, and BRAMS model outputs (Fig. 10b, d, f) for 14:00–17:00 UT, 17:00–20:00 UT, and 20:00–23:00 UT respectively, thus 30 min time-shifted with respect to the TRMM products. BRAMS outputs are displayed for Grid 1 in the whole geographical domain to be comparable to the TRMM products resolution. Panel 10a shows a large area of precipitation in central Niger with a maximum at ∼17° N, 8.5° E. Another area of precipitation is sampled in the South-East of the domain close to the Niger/Nigeria border. The corresponding BRAMS simulation (10b) shows a smaller area of precipitation in central Niger because the convective system in BRAMS develops later than in the observations. However the maximum of precipitation is located at the same place with a similar intensity. It is worth noticing that the convection triggers in a region of mountains as shown in Fig. 6. Sensitivity tests on orography parameters used in the simulation show that orography plays an important role in the convection triggering. The area of precipitation close to the Nigeria border is also reproduced by BRAMS, although it is located more West than the observations.

Around 18:00 UT the observed and modelled rainrates both indicate an intensification of the MCS North to South (close to 8° E and between 16° N and 18° N), and a westward propagation. The core of high rainrates is comparable in both cases. The area of precipitation in the South-East propagates slightly west-ward with a core of high rainrates similar in both cases but more West in BRAMS, as at 15:00 UT. Around 21:00 UT both panels 10e (TRMM) and 10f (BRAMS) show a south-westward propagation of the MCS but slower in the model. This is due to the fact that while propagating westward, the BRAMS MCS gets out of Grid 2 and enters in the Grid 1 domain where convection is determined by a subgrid scale parameterisation, coarsening the key parameters which determine the MCS lifetime and propagation speed. The Niger/Nigeria border area of precipitation propagates westward in TRMM and BRAMS. Due to the south-westward propagation of the MCS, this area converges to the MCS and later forms a unique cloud system, shown in both satellite observations and modelling. The TRMM outputs at 21:00 UT show that the activity of the MCS decays as highlighted by

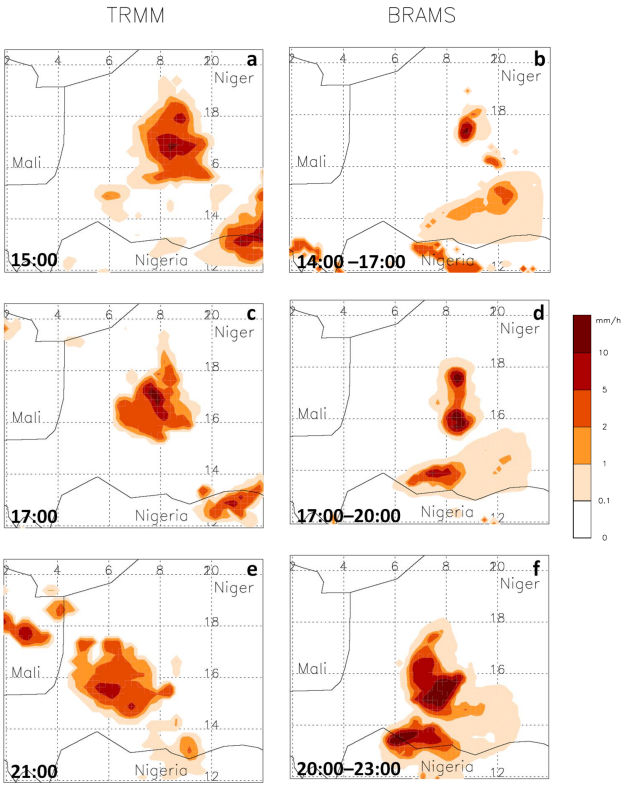

Fig. 10. Comparison between TRMM (**a, c, e**) and BRAMS (**b, d, f**) surface rainrate accumulated over 3 h periods for the Aïrcase. Panel (a): from 13:30 UT to 16:30 UT on 4 August 2006. (b) From 14:00 to 17:00 UT. Panel (c) from 16:30 to 19:30 UT. and (d) from 17:00 to 20:00 Panel (e) from 19:30 UT to 21:30 UT and (f) from 20:00 to 23:00 UT.

a maximum rainrate lower than 10 mm h^{-1} in the core of the system while BRAMS still shows a very active core. This is partially due to the fact that BRAMS outputs are 30 min later than the TRMM outputs and that the observed MCS, after a decaying phase, re-intensifies later from 23:00 UT. This time is taken into account into BRAMS in the evaluation of the rainrates but is not taken into account in the TRMM outputs of the corresponding period which ends at 22:30 UT. This also could be due to the fact that the modelled MCS is late with respect to the observed one, and thus is still active at that time.

Figure 11 illustrates the overshooting activity as seen by the BRAMS simulations within Grid 3. It shows latitude/longitude grid points having ice mass mixing ratio higher than 0.1 g kg^{-1} above the 380 K level in the time range between 18:30 UT and 21:15 UT. The threshold of 0.1 g kg^{-1} is twice the one chosen for the Chad to make Fig. 11 more readable. Figure 11 uses the same colour timescale as in Fig. 5 but shifted in time by 3 h and 15 min with respect to the BTD overshooting pixels observations. This is done to account for the time shift of the model MCS compared to observations. Panel 11b shows that the modelled MCS injects

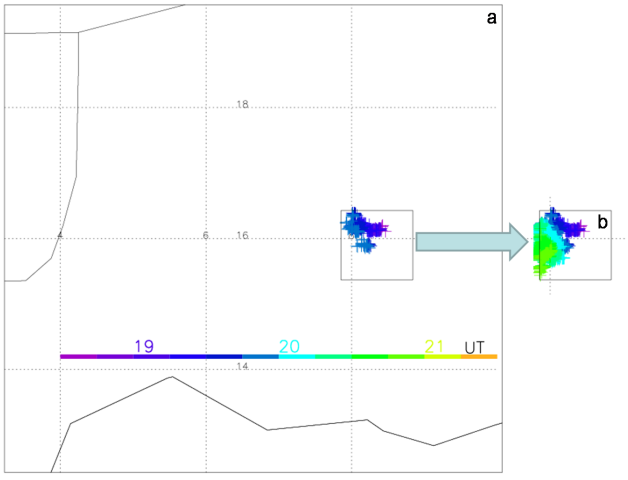

Fig. 11. Same as Fig. 8 but for the Aïr case. The same color scale as in Fig. 5 is chosen. **(a)** Zoom on Grid 3 from 18:30 to 19:50 UT. **(b)** From 18:30 UT to 21:15 UT.

ice above the tropopause during a time range similar to the overshooting observations, but later than the observed MCS. The longitude range of the modelled overshoot is also comparable with the observed one in the first 75 min (Fig. 11a). In contrast to the Chad case, the displacement of the overshooting signal in BRAMS is not only due to the horizontal advection of ice injected by the overshoot, since there are several stratospheric penetrations (first at 8.35° E, and later at 8.18° E) at 19:10 UT and at 19:45 UT in our simulation. After this time, BRAMS still produces ice injection above the tropopause but the geographical distribution of overshoots differs from the observations. Overshoots are computed in the South-West part of the Grid while the observations only show a displacement of the overshooting pixels with time from East to West-North-West. Nonetheless the overshooting time evolution is very well reproduced by BRAMS in the first 75 min of the modelled overshooting period (see results in panel 11a) with the same direction of displacement, highlighting that during this period, the overshoots in BRAMS are realistic even if late with respect to the observations. Examination of the modelled cloud top during the overshooting period shows that overshoots can reach 18.5 km (Fig. 12).

To summarize, the key parameters of the 5 August 2006 Aïr MCS (location, propagation direction, intensity of precipitation, overshooting activity) are generally well reproduced by the BRAMS simulation. Nevertheless the modelled MCS develops later than the observations and the overshooting activity is overestimated at the end of the simulation. The end of the simulation will not be taken into account in the calculation of the water fluxes across the tropopause presented in the next section.

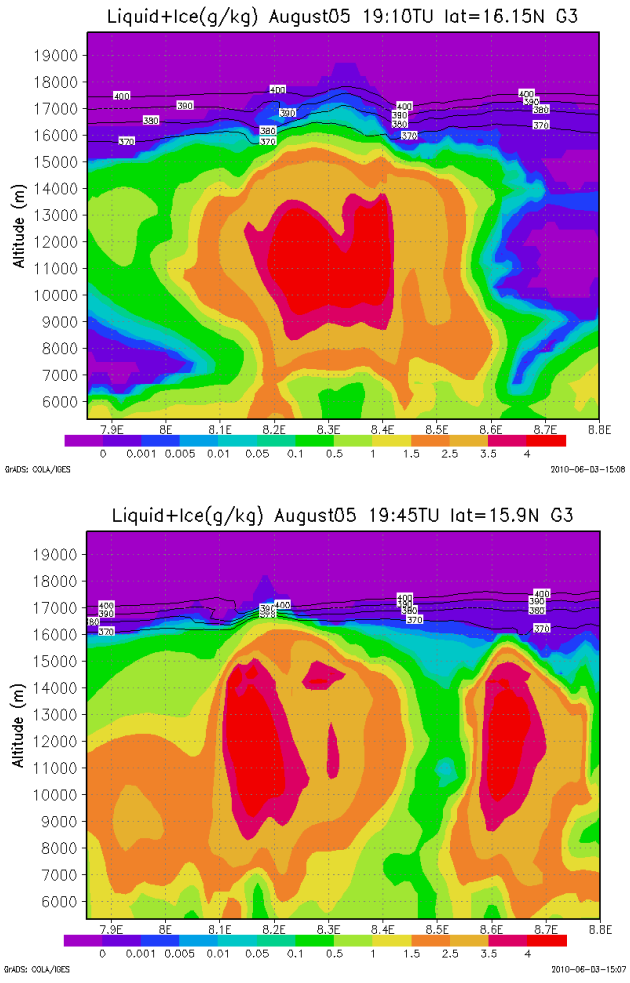

Fig. 12. Grid 3 vertical cross-section of condensed water (g kg^{-1}) for the Aïr case BRAMS simulation. Isentropic levels are also shown. **(a)** Longitude/Altitude vertical cross-section at 16.15° E latitude, at 19:10 UT. **(b)** Longitude/Altitude vertical cross-section at 15.9° E latitude, at 19:45 UT.

5 Overshooting convection and cross-tropopause water vapour transport

In Sect. 4 we have shown that the simulations performed for the two overshoot case studies are in good agreement with observations. In the following we calculate water budget across the tropopause. These two overshooting case studies are interesting to compare since they have different characteristics (organization, formation process, duration, size, intensity). The two cases described above give an opportunity in the same study to compare the impact of two different overshoots by their lifetime and area in Africa. This might be helpful to later determine a size/duration dependence of the amount of ice injected in the lower stratosphere by such extreme events.

Since the tropopause height is locally disturbed by deep convection, especially during convective events when waves generated by convection can impact the tropopause height, calculating the water flux across the tropopause needs to account for this variation. This tropopause height variation with the convective activity is highlighted in Figs. 9 and 12. Therefore the isentropic vertical coordinate should be used to locate the tropopause. Here we use the 380 K level (cf. Holton et al. 1995).

To compute the water flux across isentropic levels which are potentially moving, the vertical velocity of the θ-levels needs to be determined, so that the relative vertical wind speed with respect to the θ-levels displacement can be used. To compute the vertical speed of the θ-level, the variation of height with time of a θ-level is calculated. For this, a time-step of 5 min is used, justifying why the time frequency of BRAMS outputs are of 5 min during the overshooting period.

The total water fluxes across the θ-level are computed within the third grid of simulation through all the grid meshes with positive relative wind speed. The same technique has been applied by Chaboureau et al. (2007), but these authors have used a time-step for model outputs of 10 min instead of 5 min in our case. All variables needed for the flux calculation are interpolated in a new grid using potential temperature as vertical coordinate.

5.1 Chad case

In order to estimate the impact of overshooting convection on the water composition at mesoscale, Fig. 13 shows a Grid 3 scatter plot of UTLS total water at different times of the simulation: initial state, overshooting period, just after the overshooting period, and after convection. At 14:15 UT (panel b), the range of total water values is widely spread above the 380 K level, with some values over 100 ppmv. This is due to the decrease in the altitude of the 380 K level at that time in the vicinity of the overshooting plume as shown in Fig. 9. Values as high as 50 ppmv have been observed by the FISH instrument onboard the Geophysika M55 aircraft at 400K above the Hector cloud in the maritime continent (Corti et al., 2008; Chemel et al., 2009) on 30 November 2005. During AMMA in Africa, lower values are reported but reach sometimes 10 ppmv in filaments in the lower stratosphere (Schiller et al., 2009). In order to go a step further in the comparison with measurements associated to overshoots, the IWC was computed in the Grid 3 domain from 14:00 UT to 16:00 UT, and has been compared to measurements of stratospheric ice during TROCCINOX (Brazil) and SCOUT-O3 (Darwin, Australia) provided in Fig. 1 of Corti et al. (2008). At 390 K the BRAMS model exhibits IWC up to 10^{-3}...3.10^{-3} g m^{-3}, while Corti et al. (2008) report measurements with maximum of IWC typically of 1.5×10^{-3}...2.10^{-3} g m^{-3}, thus in the same range as ours. At about 400 K the Chad case simulation exhibits IWC up to 10^{-3}...2.10^{-3} g m^{-3}, while Corti et al. (2008) report measurements with maximum of

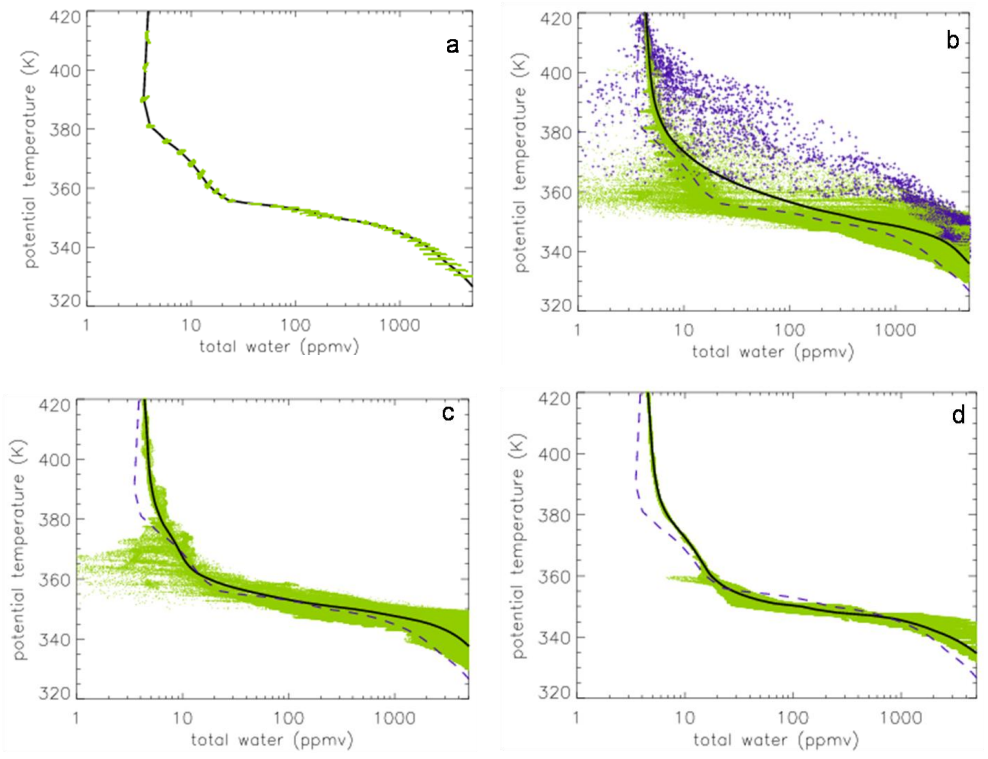

Fig. 13. Scattergram of total H_2O/potential temperature within the Grid 3 domain of BRAMS at different times of the simulation for the Chad case. **(a)** Initial state at 18:00 UT on 3 August. **(b)** 14:15 UT on 4 August at the maximum of the overshooting activity. **(c)** 15:55 UT after the overshooting activity. **(d)** 21:00 UT after the convective activity. The black solid line is the mean mixing ratio within the grid. The blue dashed line is the initial mean mixing ratio. Purple crosses highlight grid points in the overshooting plume area (latitude from 11.95° N to 12.06° N and longitude from 20.9° E to 21.1° E).

IWC typically of $1.10^{-3}...3.10^{-3}$ g m^{-3}. At this level, more cases have been sampled than at 390 K in Corti et al. (2008). Again, the measured and the observed IWCs are comparable. Between 400 and 410 K most of the BRAMS grid meshes containing ice have IWC in the range 10^{-4} to 10^{-3} g m^{-3}. In Corti et al. (2008), in the 400 K–420 K range, the same IWC values are reported but the maximum IWC values are generally higher than for BRAMS. From this it can be concluded that, although the IWC measurements reported in Corti et al. (2008) are from a different continent than Africa and cannot be directly compared with our simulation, the stratospheric IWCs computed by BRAMS are of the same order of magnitude and confirm that our overshoot simulation is realistic.

In Fig. 13b purple crosses highlight grid points in the overshooting plume area (latitude from 11.95° N to 12.06° N and longitude from 20.9° E to 21.1° E). They show that most of the high water mixing ratios in the stratosphere are due to this overshoot, enhancing the water amount of 2 to 3 ppmv above the 400 K level.

Important to notice is that the mean profile at 14:15 UT is higher at any altitude than the initial profile, showing a mean hydration at all level. The same conclusion is reached when comparing the pre-overshoot mean profile at 12:00 UT on 4 August and the mean profile at 14:15 UT. After the overshooting activity (panel c) stratospheric water values are less scattered than during the overshoot. But there is still a local enhancement of 2 ppmv with respect to the mean profile between 380 and 390 K. A striking feature of panel b and c is the scatter of the very low water mixing ratios in the TTL below the tropopause, showing that deep convection can also lead to dehydration in the upper troposphere. This tendency is visible in the mean profile at 15:55 UT where it is lower than the initial state in the TTL from 360 K to 370 K. It is not seen at 14:15 UT since deep convection leads to a local large hydration that influences the mean profile. When convection disappears from Grid 3 (21:00 UT), there is almost no variation of the water amount in the stratosphere, even if the mean profile remains significantly higher than the initial one. Above the tropopause, the mean profile is typically 0.21 ppmv at 400 K to 0.67 ppmv at 380 K higher than the pre-overshoot mean profile at 12:00 UT between 380 and 400 K. In the modelling study of overshooting convection above the Hector Cloud (maritime continent) using the ARW model, Chemel et al. (2009) report an estimation of 0.12 ppmv water increase in the 405–410 K range This

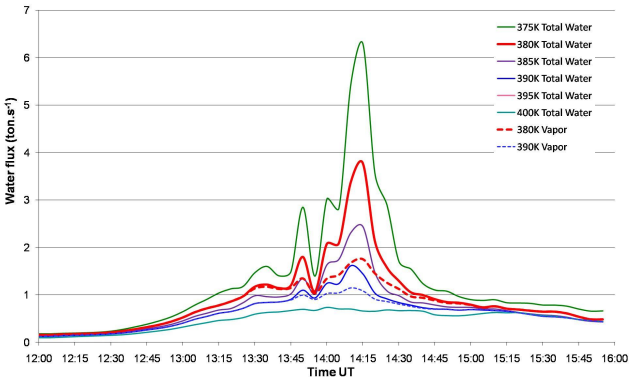

Fig. 14. Upward total water flux across different isentropic levels within the BRAMS Grid 3 domain between 12:00 UT and 15:55 UT for the Chad case. For the 380 K and 390 K isentropic levels, the water vapour flux are also shown (dashed line).

0.12 ppmv value corresponds to the maximum mean increase out of all the increases computed every 5 K up to 425 K. This number is not directly comparable with the one given in the present study since the size domain of the ARW simulation is 341×341 km, that is 4.94 times our domain size (214×110 km). Thus the relatively low number of Chemel et al. (2009) is balanced by a larger domain. In Grosvenor et al. (2007) an idealized overshooting case over Brazil is discussed. They report a mean moistening of ∼0.3 ppmv above the tropopause in the 16–17 km range for the most vigorous case of Grosvenor et al. (2007) with a domain size of 150 × 150 km which is very close to the size of the present study. Thus, this 0.3 ppmv increase is comparable with the mixing ratio enhancement presented in the present study. Note also that the Unified Model simulation of the Hector cloud also presented in Chemel et al. (2009) which highlights a 5–6 ppmv increase in the range 410–415 K for a larger domain (240×240 km). This estimation is clearly higher than for the Chad case.

Water fluxes of the Chad case are calculated for the most active period in Grid 3 from 12:00 UT to 16:00 UT on 4 August 2006. Figure 14 presents the times series of upward total water flux through isentropic surface from 375 K to 400 K. For all levels except 400 K several peaks are found at 13:50 UT, 14:00 UT and 14:15 UT. They correspond well to the time of overshooting plumes in Grid 3, as shown in Fig. 9 for 14:15 UT. The overshooting signal is not obvious at the 400 K level. This can be explained by the fact that the overshooting plumes shown in Fig. 9 cross the 400 K level in a more limited area and that the ice mixing ratios are lower, in contrast to lower θ-levels. Focusing on the tropopause level (380 K), the maximum instantaneous flux is of 3.77 ton s^{-1}, which is 3 times less than for the 370 K (not shown) and 1.66 times less than for the 375 K level. At the same time, note the instantaneous flux of more than 1 ton s^{-1} across the 395 K level. After 14:15 UT, the instantaneous fluxes decrease rapidly to tend to the same value at levels higher than 375 K when overshoot activity has disappeared in Grid 3, to tend later to zero.

In order to compare our result with Chaboureau et al. (2007), upward fluxes for water vapour only at 380 K and 390 K are reported in Fig. 14. At the maximum of the overshooting activity the water vapour flux at 380 K is 2.15 times the total water flux with a value of 1.75 ton s^{-1}. This confirms that ice injection above the tropopause is a key element of the amount of water entering the stratosphere. However the water vapour contribution is far from negligible. In Chaboureau et al. (2007), the water upward flux reported is 9 ton s^{-1} for the same isentropic level (380 K). At 390 K they report an 8 ton s^{-1} while it is 1.14 ton s^{-1} in the present study. Keeping in mind that in Chaboureau et al. (2007) the domain of calculation is 2.66 larger than in the present study, the differences highlighted here should be moderated: expressed in the same surface area as for the Chad case, the Chaboureau et al. (2007) fluxes would be 3.38 ton s^{-1} at 380 K and 3 ton s^{-1} at 390 K. Thus our calculations are compatible with the one of Chaboureau et al. (2007) with the same order of magnitude in the water modelling fluxes of typically a few tons per second. However our maximum estimation is still lower. This might be due to the use in our study of a double moment microphysical scheme and a budget calculation time step of 5 min instead of a single moment scheme. Marécal et al. (2010) have shown in a convective cell simulation that the amount of ice of the cell core was higher for a single moment microphysical scheme than for a similar simulation using a double moment microphysical scheme. Another possible explanation is a difference in the vertical velocities computed in each simulation. During the overshoot, the BRAMS simulation exhibits maximum values of typically 25 m s^{-1} with a peak value of 29 m s^{-1} at 14:00 UT, in contrast with the 75 m s^{-1} and 60 m s^{-1} reported in Chaboureau et al. (2007) which may not be realistic. Finally we have checked the influence of the time resolution to compute the fluxes on isentropic levels by choosing the same 10 min resolution as in Chaboureau et al. (2007). No important difference appears with the 5 min time step calculation.

Integrated over the 4 h period covering the overshooting event and on the surface area of Grid 3, the mass of total water crossing upward the θ-levels are given in Table 3. The corresponding numbers per unit of time are also given. For the 380 K level which corresponds to the tropopause, a total mass of water of ∼13 kton has crossed this level during the 4 h period. This corresponds to a mean value of ∼3300 ton h^{-1} or 0.91 ton s^{-1}. This computation does not take into account potential removal of ice crystal by sedimentation. However, the total water relative humidity with respect to ice computed by BRAMS highlights generally unsaturated conditions (<80%) in the LS, except a local maximum of 110% at 14:20 UT at 17 km. These conditions provide sublimation of ice crystal before they can be totally

Table 3. Water budget associated to the overshooting convection for the Chad and the Aïr cases across different isentropic surfaces. The integrated flux is the total mass of water crossing the θ levels upward during the integration period covering the overshoot (4 h for the Chad case and 1h 50 min for the Aïr case). Also shown are the same results divided by the period of integration. The lower limit and the upper limit of the mass of water injected by the overshoot which remains in the stratosphere after the ice disappears are given for each case.

Cases	Isentropic levels (K)	370 K	375 K	380 K	385 K	390 K	395 K	400 K	Extra mass of water after the overshoot (tons)
Chad	Integrated flux (ton)	29 558	18 171	13 107	10 581	8963	7726	6841	Upper limit: 507
	Per unit time (ton h^{-1})	7389	4542	3276	2645	2240	1931	1710	Lower limit: 330
	Per unit time (ton s^{-1})	2.1	1.3	0.9	0.7	0.6	0.5	0.5	
Aïr	Integrated flux (ton)	12 172	6313	4332	3465	2966	2677	2471	Upper limit: 200
	Per unit time (ton h^{-1})	6639	3443	2363	1890	1618	1460	1348	
	Per unit time (ton s^{-1})	1.8	0.9	0.7	0.5	0.4	0.4	0.4	

removed from the lower stratosphere by sedimentation. Nevertheless, ice particles do not sublimate instantaneously so that this process could lead to a significant loss of water in the stratosphere as suggested by Corti et al. (2008): the budget computed here should be seen as an upper limit.

In order to estimate the amount of overshot water that remains in the stratosphere, the mass of water between the 380 K and 410 K levels (the highest levels where the ice penetrates) was computed in the grid 3 domain from 12:00 UT to 16:00 UT (see Fig. 15). A reference value of zero was set at the time when ice starts to appear in Grid 3 since the aim is to characterise the stratospheric water mass change due to the overshoot alone and not to the whole convective system. Figure 15 shows from 13:30 UT a regular increase of water vapour followed by a sharp increase in stratospheric ice mass. A local maximum is reached at 14:00 UT due to a maximum of ice mixing ratio. The corresponding total overshot water is about 600 tons. This is followed by a decrease, mainly due to ice sedimentation, the amount of water vapour remaining constant. The overshot water mass reaches its maximum ($\sim$800 tons) at 14:20 UT shortly after the convection is the most severe. From this time ice decreases while water vapour slightly increases due to ice sublimation. The loss of ice is caused by both sedimentation and sublimation. From 14:50 UT when the stratospheric hydrated plume starts to exit the grid 3 domain horizontally, the extra overshot mass decreases more sharply. This does not mean a loss of mass for the stratosphere. From this time, several hypotheses are made to estimate the amount of water that will remains in the stratosphere once all the ice has disappeared. Keeping in mind that the stratosphere is under-saturated with respect to ice at locations where ice remains, it is unlikely that significant water vapour loss occurs by condensation on ice. The amount of overshot water which remains in the stratosphere should be contained between two cases. (1) Assuming a constant water vapour concentration, we assume that all the stratospheric ice sediment without sublimating. This is shown in bold lines in Fig. 15, using the amount of ice computed from a sub-domain of Grid 2 which includes the hydrated plume from the overshoot. In this domain, no other source of stratospheric ice is included. This hypothesis leads to a remaining extra mass of water of $\sim$330 tons. (2) Contrarily to (1), we assume that all the ice sublimates without having the time to sediment. This is shown in bold lines with plus marks in Fig. 15. It leads to an amount of water of 507 tons. Neither of these hypotheses is realistic but it is

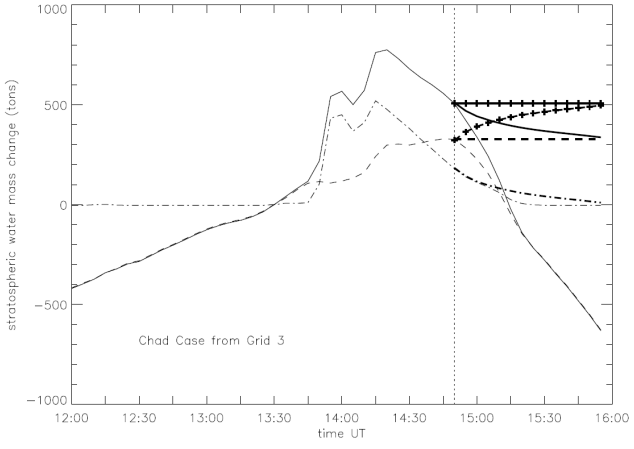

Fig. 15. Stratospheric water mass change associated to the Chad case overshoot computed from Grid 3 (thin lines) between the 380 K and the 410 K levels. Total water (solid line), water vapour (dashed line), and ice (dotted-dashed line) are shown. The reference value is set to zero when ice starts to appear in the stratosphere. The vertical dotted line at 14:50 UT indicates that the hydrated signal in the stratosphere starts to exit from grid 3. From this time, the use of several hypotheses is shown in thick lines. The dashed-dotted thick line is ice mass change computed in Grid 2. The thick dashed line assumes a constant vapour amount from 14:50 UT (no sublimation of ice that is finally completely removed by sedimentation). The thick solid line is the sum of the corresponding thick vapour and ice lines. The thick lines with "plus" marks assume that all the ice sublimates into vapour without any loss by sedimentation.

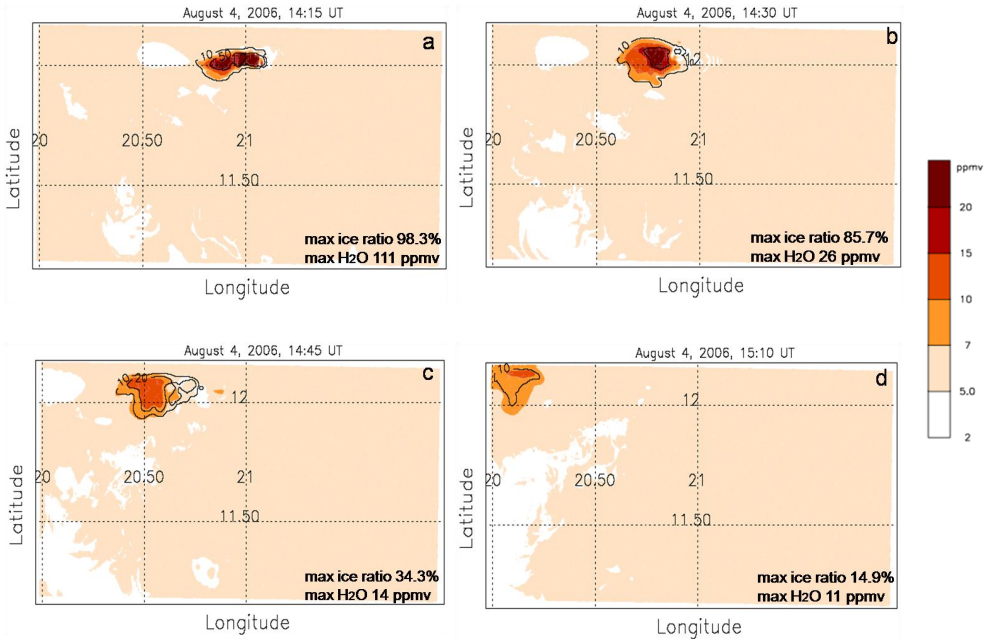

Fig. 16. Total water at the 390 K isentropic level in the BRAMS Grid 3 domain at 14:15 UT **(a)**, 14:30 UT **(b)**, 14:45 UT **(c)** and 15:10 UT **(d)** for the Chad case simulation. Also shown are contours of ratio (%) of ice with respect to total water (black solid lines): (a) and (b) 10% and 50%, (c) 10% and 20%, and (d) 10%. The maximum total water mixing ratios as well as the maximum ratio (%) of ice with respect to total water are reported in each panel. The same colour scale applies to each panel.

likely that they give the range of water that remains in the stratosphere, from 330 to 507 tons. These values are compatible with the values given by Grosvenor (2010), from the simulations reported in Grosvenor et al. (2007): his estimation is between 100 tons (weak case) and 1100 tons (vigorous case) depending on the severity of the overshoot. Recently, based on measurements from the A-Train constellation above the warm pool region, Iwasaki et al. (2010) estimated the overshot mass that remains in the stratosphere to 100 tons. Although the estimation we give is of the same order of magnitude, our case is at least 3 times higher. However, these estimations are seldom in the literature, and it is not possible to say what estimation is the most representative of a typical overshoot.

Figure 16 shows the time evolution of the total water at the 390 K isentropic levels in the Grid 3 domain from the time of the most severe overshoot (14:15 UT). It shows that the hydrated signal is advected with the wind for one hour in Grid 3. While travelling westward, the signal spreads North and South and the maximum of total water decreases due to horizontal diffusion, and possibly vertical diffusion and sedimentation of large ice particles. Fig. 16 also shows that the ratio of ice to the total water decreases with time while the area of maximum hydration travels westward. It varies at the maximum from ∼98% at 14:15 UT to ∼15% at 15:10 UT, showing that despite of slightly subsaturated conditions with respect to ice, ice particles remains in the lower stratosphere one hour after the overshoot. Before going out of Grid 3, the area of maximum hydration is still 3 ppmv higher than the background water content at the maximum (10.2 ppmv at 15:20 UT), 1 h and 5 min after the overshoot, ∼100 km away from it. Note that the maximum of total water decreases with time from the time of the overshoot to the time when the hydrated spot goes out of the Grid 3 domain. Despite a change in the horizontal resolution from 1 km to 4 km, the signal is still advected trhough Grid 2 until 16:00 UT. In Grid 2, the total water decrease with time is relatively slow long after the overshoot. This indicates that a local enhancement of stratospheric water due to overshooting can travel relatively far from the overshoot. The maximum value at 15:55 UT is slightly lower but close to 2 ppmv higher than the background level. This is compatible with the K2009 hypothesis which explains that the local enhancement of water vapour above Niamey is due to the overshooting convection of the Chad system. This hydrated bulge has also been followed in the Grid 1 domain with the coarser horizontal resolution (20 km). When the simulation ends, the hydrated signal is above the Chad/Cameroun/Nigeria border with a maximum mixing ratio ∼0.7 ppmv higher than the environment. This value is relatively low compared to the hydrated layer observed by micro-SDLA and FLASH. However we cannot rule out an effect of the coarse resolution which would spread the overshot plume too fast.

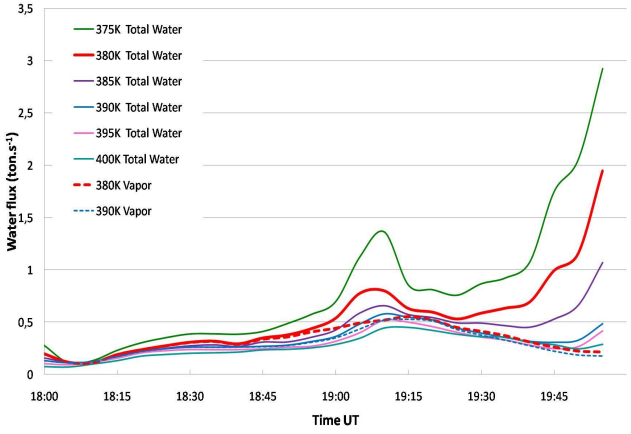

Fig. 17. Same as Fig. 14 but for the Aïr case, computed between 18:00 UT and 19:50 UT on 5 August 2006.

5.2 Aïr case and comparison with the Chad case

Similar calculations were carried out for the case of August 5. The period of 18:00 UT to 19:50 UT has been used to compute water fluxes across different isentropic levels in the grid 3 domain. We limit our calculation to this period in order to keep only the period when there is a good agreement between the MSG overshooting activity and the BRAMS overshooting activity (see Sect. 4.2). The results are given in Fig. 17 and flux values are summarized in Table 3. A two peak structure is shown in Fig. 17, highlighting two different short periods of intense overshooting convection. The first peak, at 19:10 UT, is visible for all θ-levels showing that overshooting convection directly injects ice particles above the 400 K, as shown in Fig. 12. At 380 K, this peak reaches a maximum of 1.1 ton s^{-1} for total water, with a corresponding flux for water modelling of 0.56 ton s^{-1} (more than half the total flux), which is less than the peak described for the Chad case. The latter number should be compared with the flux calculation of Chaboureau et al. (2007), multiplied by the surface area ratio of each simulation ($106\times118/250\times250$=0.2), that is 1.8 ton s^{-1} at 380 K and 1.6 ton s^{-1} at 390 K. Again, the calculations of Chaboureau et al. (2007) are higher than ours. The second peak, at the end of the calculation period, reaches a higher value of 1.49 ton s^{-1} that is still lower than for the Chad case. The difference is likely due to the smaller surface area of overshoots for the Aïr case. Note for the second peak that the overshooting signal is not seen at the 390 K level and above. This illustrates that this overshoot penetrates those levels on smaller surface area that for the Chad case. The integrated fluxes during the whole period given in Table 3 highlight lower values per unit of time than for the Chad case, though the Aïr case is shorter in duration. For θ-levels in the stratosphere ($\geq$380 K), the Aïr case budget is typically 0.75 times the Chad budget. This shows the variability of the impact of overshooting convection on the amount of water injected in the stratosphere among the cases.

The same stratospheric water mass change calculation has been applied to the Aïr case as for the Chad case. However, considering the discrepancies between the model and the BTD observation from 19:50 UT when the model overestimates the overshooting activity, it is not possible to study the evolution of the stratospheric hydrated plume. Contrarily to the Chad case, the overshooting convection led to a strong increase of ice (800 t at 19:00 UT) but was associated to a loss of water vapour in the surrounding, so that the total water increase at 19:50 UT is less than 200 tons. This number has to be compared with the 800 tons of total water which are reached at maximum of the Chad case. We cannot conclude about the water amount that remains in the stratosphere but it is clear that the Chad case hydrates significantly more the stratosphere than the Aïr case. Even assuming that the 200 tons of water would remain in the stratosphere, which is likely not true, there would be at least a factor of two third between the Aïr and the Chad case. This highlights once again that depending on the case studied, the impact on the stratosphere hydration is significantly different. One of the reasons for the difference between the Aïr and the Chad cases is the difference with respect to the saturation: the Chad case occurs in a dryer environment than the Aïr case. In the Aïr case, while injecting total water in the stratosphere, the saturation with respect to ice is reached in small area in the surrounding of the overshoot for all time considered at 380 K. Water vapour condenses on ice particles which fall out. Consequently, the modelled stratospheric water mass tends to decrease shortly after the overshoot. Concurrently for the Chad case, it was checked that the RHi was lower than 100% in the overshot plume. Thus ice particles tend to evaporate.

6 Conclusions

The aim of this study was to quantify the impact of two different overshooting events on the water budget in tropical tropopause region during the African monsoon 2006. One of these events was directly upstream of a pair of balloon flights from Niamey measuring water vapour in the UTLS in the frame of the SCOUT-AMMA campaign. During these flights a layer of enhanced water vapour of more than 2 ppmv was measured. Three nested grids regional down to cloud resolving simulations were conducted with the BRAMS model. A double moment bulk microphysical scheme is used in our simulation. This study confirms previous estimates from model simulations that overshooting convection injects a large amount of water via ice crystals which later sublimate in a sub saturated environment, while sedimenting. However, our water modelling flux estimation is lower than the one of Chaboureau et al. (2007) who studied an overshoot over Brazil. This could be due to the use of a double moment scheme in BRAMS in contrast with the single moment scheme of meso-NH: single moment schemes are known to overestimate precipitation and the concentration of ice

crystals with respect to double moment schemes which are more precise. For the case of 4 August 2006 over Southern Chad, a total amount of 13 kton is injected into the stratosphere leading locally to an enhancement of total water of 3 ppmv at 400 K and to mixing ratios higher than 100 ppmv at the tropopause. At a regional scale, after the overshoot, the mean water amount in the Grid 3 domain above the tropopause is still enhanced by 0.21 ppmv at 400 K to 0.67 ppmv at 380 K. This result is comparable with the 0.3 ppmv water enhancement given in an overshoot study in Brazil by Grosvenor et al. (2007) for a similar domain size, and is compatible with the ARW model simulated enhancement of 0.12 ppmv for Hector in Northern Australia (Chemel et al., 2009), in which the model size is larger than ours, making a direct comparison difficult. In the above mentioned study the water enhancement given by the UM model simulation is much larger (5.91 ppmv) than is the present work. This highlights the variability among mesoscale models to simulate the hydration of the lower stratosphere by deep convection, together with the variability of the impact of overshoots depending on the continent considered. But whatever this variability is, all these modelling studies conclude to a potential of overshooting convection to hydrate the LS.

A mass of extra total water that remains in the stratosphere after the overshoot was computed: a range of 330 to 507 tons was found, in the range of various estimations (100 to 1100 tons) given by Grosvenor (2010). Our calculation is higher than the estimation of 100 tons deduced from satellite observations (Iwasaki et al., 2010).

After being advected for more than one hour and ∼100 km away from the overshoot, the hydrated area at the 390 K level is still 3 ppmv higher than the background water amount, showing that the impact of the overshoot can be seen far away from its location. Thus, it is likely that the water vapour enhancement of more than 2 ppmv sampled by FLASH-B and micro-SDLA on 5 August above Niamey is due to overshooting convection over South Chad 30 h earlier, as proposed by Khaykin et al. (2009).

Another more organised overshooting system was studied over Aïr and the associated water budget across the tropopause was computed. It shows a total mass of water injected in the stratosphere 3 times lower than for the Chad system, though the Aïr case is shorter. The difference is less but still significant when the result is expressed per unit of time: 0.66 ton s^{-1} for the Aïr case instead of 0.91 ton s^{-1} for the Chad case. Our estimation of the water mass amount which remains in the stratosphere after the overshoot (at the most 200 tons) is two thirds that calculated for the Chad case for the most favourable estimation. This shows the variability of the impact of overshooting convection on the hydration potential of the stratosphere, which was not highlighted in previous studies.

The relative impact of overshooting convection with respect to the cold trap dehydration is not assessed yet. The impact of such mesoscale hydration at a larger space and time scales needs to be studied first, in order to reconcile the small scale and the larger scale H_2O transport pathways which are still highly debated. We propose as a first step to better estimate the variability of the impact of overshooting convection among a larger set of different cases and different type of overshooting convection. We also propose to check the impact of key parameters in the model such as the microphysical scheme or the model resolutions to pinpoint the reasons for the differences among models on the LS hydration. Concurrently, it would be interesting in the future to compare water budgets of the same case but with different mesoscale models. From this, typical impact of overshoots could be obtained and be included in larger scale models to upscale the impact of overshooting convection on the whole tropical lower stratosphere.

Acknowledgements. This work was supported by the European integrated project SCOUT-O3 (GOCE-CT-2004-505390) and by the program LEFE/INSU in France (projects UTLS-tropicale and Tropopause 2009). The computer resources were provided by CRIHAN (Centre de Ressource Informatique de Haute Normandie) project n° 2008006 .This work was also granted access to the HPC resources of CINES under the allocation 20080125036 and 2009015036 made by GENCI (Grand Equipement National de Calcul Intensif). The TRMM data were provided by GSFC/DAAC, NASA. The CALIPSO/CALIOP image was distributed by Atmospheric Science Data Center, at NASA Langley Research Center. Meteosat Second Generation data were provided by the AMMA database and the Climserv database at Institut Pierre Simon Laplace (IPSL). One of the authors, Xiaoman Liu is funded by Région Champagne-Ardenne. G. Pénide and V. Giraud at Laboratoire de Météorologie Physique (LaMP) are ackowledged for their advices in the BRAMS setting. We wish to acknowledge D. Grosvenor whose comments helped to improve the manuscript. Finally, we are grateful to the micro-SDLA technical team of DT-INSU (N. Amarouche, F. Blouzon and J. Deléglise) for their investment during the SCOUT-AMMA campaign in Niamey.

Edited by: N. Harris

The publication of this article is financed by CNRS-INSU.

References

Agusti-Panareda, A., Beljaars, A., Cardinali, C., Genkova, I, and Thorncroft, C.: Impact of assimilating AMMA soundings on ECMWF analyses and forecasts, Weather Forecast, 25(4), 1142–1160, 2010.

Agusti-Panareda, A., Vasiljevic, D., Beljaars, A., Bock, O., Guichard, F., Nuret, M., Garcia Mendez, A., Anderson, B. E.,

Bechtold, P., Fink, A., Hersbach, H., Lafore, J.-P., Ngamini, J.-B., Parker, D. J., Redelsperger, J.-L., and Tompkins, A. M.: Radiosonde humidity bias correction over the West African region for the special AMMA reanalysis at ECMWF, Q. J. Roy. Meteorol. Soc., 135, 595–617, 2009.

Cairo, F., Pommereau, J. P., Law, K. S., Schlager, H., Garnier, A., Fierli, F., Ern, M., Streibel, M., Arabas, S., Borrmann, S., Berthelier, J. J., Blom, C., Christensen, T., D'Amato, F., Di Donfrancesco, G., Deshler, T., Diedhiou, A., Durry, G., Engelsen, O., Goutail, F., Harris, N. R. P., Kerstel, E. R. T., Khaykin, S., Konopka, P., Kylling, A., Larsen, N., Lebel, T., Liu, X., MacKenzie, A. R., Nielsen, J., Oulanowski, A., Parker, D. J., Pelon, J., Polcher, J., Pyle, J. A., Ravegnani, F., Rivire, E. D., Robinson, A. D., Röckmann, T., Schiller, C., Simões, F., Stefanutti, L., Stroh, F., Some, L., Siegmund, P., Sitnikov, N., Vernier, J. P., Volk, C. M., Voigt, C., von Hobe, M., Viciani, S., and Yushkov, V.: An introduction to the SCOUT-AMMA stratospheric aircraft, balloons and sondes campaign in West Africa, August 2006: rationale and roadmap, Atmos. Chem. Phys., 10, 2237–2256, doi:10.5194/acp-10-2237-2010, 2010.

Chaboureau, J.-P., Cammas, J.-P., Duron, J., Mascart, P. J., Sitnikov, N. M., and Voessing, H.-J.: A numerical study of tropical cross-tropopause transport by convective overshoots, Atmos. Chem. Phys., 7, 1731–1740, doi:10.5194/acp-7-1731-2007, 2007.

Chemel, Ch., M. Russo, J. A. Pyle, R. S. Sokhi, and C. Schiller: Quantifying the imprint of a sever Hector thunderstorm during ACTIVE/SCOUT-O3 onto the water content in the upper troposphere/lower stratosphere, Mon. Weather Rev., 103, 2493–2514, doi:10.1175/2008MWR2666.1, 2009.

Corti, T., Luo, B. P., de Reus, M., Brunner, D., Cairo, F., Mahoney, M. J., Martucci, G., Matthey, R., Mitev, V., dos Santos,F. H., Schiller, C., Shur, G., Sitnikov, N. M., Spelten, N., Vossing, H. J., Borrmann, S., and Peter, T.: Unprecedented evidence for overshooting convection hydrating the tropical stratosphere, Geophys. Res. Lett., 35, L10810, doi:10.1029/2008GL033641, 2008.

Cotton, W. R., Pielke Sr., R. A., Walko, R. L., Liston, G. E., Tremback, C. J., Jiang, H., McAnelly, R. L., Harrington, J.-Y., Nicholls, M. E., Carrio, G. G., and McFadden, J. P.: RAMS 2001: Current status and future directions, Meteorol. Atmos. Phys., 82, 5–29, doi:10.1007/s00703-001-0584-9, 2003.

Durry, G., Amarouche, N., Zéninari, V., Parvitte, B., Lebarbu, T., and Ovarlez, J.: In situ sensing of the middle atmosphere with balloonborne near-infrared laser diodes, Spectrochim. Acta, 60(4), 3371–3379, 2004.

Freitas, S. R., Longo, K. M., Silva Dias, M. A. F., Chatfield, R., Silva Dias, P., Artaxo, P., Andreae, M. O., Grell, G., Rodrigues, L. F., Fazenda, A., and Panetta, J.: The Coupled Aerosol and Tracer Transport model to the Brazilian developments on the Regional Atmospheric Modeling System (CATT-BRAMS) – Part 1: Model description and evaluation, Atmos. Chem. Phys., 9, 2843–2861, doi:10.5194/acp-9-2843-2009, 2009.

Fueglistaler, S., Wernli, H., and Peter, T.: Tropical troposphere-to-stratosphere transport inferred from trajectory calculations, J. Geophys. Res., 109, D03108, doi:10.1029/2003JD004069, 2004.

Fueglistaler, S., Bonazzola, M., Haynes, P. H., and Peter, T.: Stratospheric water vapour predicted from Lagrangian temperature history of air entering the stratosphere in the tropics, J. Geophys. Res., 110, D08107, doi:10.1029/2004JD005516, 2005.

Fueglistaler, S., Dessler, A. E., Dunkerton, T. J., Folkins, I., Fu, Q., and Mote, P. W.: The tropical tropopause layer, Rev. Geophys., 47, RG1004, doi:10.1029/2008RG0002672009, 2009.

Gettelman, A., Salby, M. L., and Sassi, F.: The distribution and influence of convection in the tropical tropopause region, J. Geophys. Res., 107, 4080, doi:10.1029/2001JD001048, 2002.

Grell, G. A. and Devenyi, D.: A generalized approach to parameterizing convection combining ensemble and data assimilation techniques, Geophys. Res. Lett., 29, 1693, doi:10.1029/2002GL015311, 2002.

Grosvenor, D. P., Choularton, T. W., Coe, H., and Held, G.: A study of the effect of overshooting deep convection on the water content of the TTL and lower stratosphere from Cloud Resolving Model simulations, Atmos. Chem. Phys., 7, 4977–5002, doi:10.5194/acp-7-4977-2007, 2007.

Grosvenor, D.: Interactive comment on "Water vapour budget associated to overshoots in the tropical stratosphere: mesoscale modelling study of 4–5 August 2006 during SCOUT-AMMA" by X. M. Liu et al., Atmos. Chem. Phys. Discuss., 10, C1348–C1351, 2010.

Harrington, J. Y.: The effects of radiative and microphysical processes on simulated warm and transition season Arctic stratus, PhD Diss., Atmospheric Science Paper N° 637, Colorado State University, Department of Atmospheric Science, Fort Collins, CO 80523, 289 pp., 1997.

Holton, J., Haynes, P., McIntyre, M., Douglass, A., Rood, R., and Pfister, L.: Stratosphere-Troposphere Exchange, Rev. Geophys., 33(4), 403-439, 1995.

Holton, J. R. and Gettelman, A.: Horizontal transport and the dehydration of the stratosphere, Geophys. Res. Lett., 28, 2799–2802, 2001.

Huffman, G. J., Adler, R. F., Bolvin, D. T., Gu, G., Nelkin, E. J., Bowman, K. P., Hong, Y., Stocker, E. F., and Wolff, D. B.: The TRMM multi-satellite precipitation analysis: quasi-global, multi-year, combined-sensor precipitation estimates at fine scale, J. Hydrometeor, 8(1), 38–55, 2007.

Iwasaki, S., Shibata, T., Nakamoto, J., Okamoto, H., Ishimoto, H., and Kubota, H.: Characteristics of deep convection measured by using the A-train constellation, J. Geophys. Res., 115, D06207, doi:10.1029/2009JD013000, 2010.

James, R., Bonazzola, M., Legras, B., Surbled, K., and Fueglistaler, S.: A Lagrangian analysis of a the Asian Monsoon Water Vapour Maximum at 110 hPa, Geophys. Res. Lett., 35, L20810, doi:10.1029/2008GL035441, 2008.

Jones, A., Urban, J., Murtagh, D. P., Eriksson, P., Brohede, S., Haley, C., Degenstein, D., Bourassa, A., von Savigny, C., Sonkaew, T., Rozanov, A., Bovensmann, H., and Burrows, J.: Evolution of stratospheric ozone and water vapour time series studied with satellite measurements, Atmos. Chem. Phys., 9, 6055–6075, doi:10.5194/acp-9-6055-2009, 2009.

Khaykin, S., Pommereau, J.-P., Korshunov, L., Yushkov, V., Nielsen, J., Larsen, N., Christensen, T., Garnier, A., Lukyanov, A., and Williams, E.: Hydration of the lower stratosphere by ice crystal geysers over land convective systems, Atmos. Chem. Phys., 9, 2275–2287, doi:10.5194/acp-9-2275-2009, 2009.

Liu, C. and Zipser, E. J.: Global distribution of convection penetrating the tropical tropopause, J. Geophys Res., 110(D23), D23104, doi:10.1029/2005JD006063, 2005.

Marécal, V., Durry, G., Longo, K., Freitas, S., Rivière, E. D., and

Pirre, M.: Mesoscale modelling of water vapour in the tropical UTLS: two case studies from the HIBISCUS campaign, Atmos. Chem. Phys., 7, 1471–1489, doi:10.5194/acp-7-1471-2007, 2007.

Marécal, V., Pirre, M., Rivière, E. D., Pouvesle, N., Crowley, J. N., Freitas, S. R., and Longo, K. M.: Modelling the reversible uptake of chemical species in the gas phase by ice particles formed in a convective cloud, Atmos. Chem. Phys., 10, 4977–5000, doi:10.5194/acp-10-4977-2010, 2010.

Meyers, M. P., Walko, R. L., Harrington, J. Y., and Cotton, W. R., New RAMS cloud microphysics parameterization. Part II: The two-moment scheme, Atmos. Res., 45, 3–39, 1997.

Nielsen, J. K., Larsen, N., Cairo, F., Di Donfrancesco, G., Rosen, J. M., Durry, G., Held, G., and Pommereau, J. P.: Solid particles in the tropical lowest stratosphere, Atmos. Chem. Phys., 7, 685–695, doi:10.5194/acp-7-685-2007, 2007.

Oltmans, S. J., Vömel, H., Hofmann, D. J., Rosenlof, K. H., and Kley, D.: The increase in stratopsheric water vapour from balloonborne frostpoint hygrometer measurements at Washington DC, and Boulder, Colorado, Geophys. Res. Lett., 27, 3453–3456, 2000.

Pénide, G., Giraud, V., Bouniol, D., Dubuisson, P., Duroure, C., Protat, A., and Cautenet, S.: Numerical Simulation of the 7 to 9 September 2006 AMMA mesoscale convective system: Evaluation of the Dynamics and Cloud Microphysics using Synthetic observations, Q. J. Roy. Meteor. Soc., 136, 304–322, 2010.

Pommereau, J.-P. and Held, G.: Is there a stratospheric fountain?, Atmos. Chem. Phys. Discuss., 7, 8933–8950, doi:10.5194/acpd-7-8933-2007, 2007.

Randel, W. J., Wu. F., Gettelman. A., Russell. J. M., Zawodny. J. M.. and Oltmans. S. J.: Seasonal variation of water vapour in the lower stratosphere observed in Halogen Occultation Experiment data, J. Geophys. Res., 106, 14313–14326, 2001.

Randel, W. J., Wu, F., Vömel, H., Nedoluha, G. E., and Forster, P.: Decreases in stratospheric water vapor after 2001: Links to changes in the tropical tropopause and the Brewer-Dobson circulation, J. Geophys. Res., 111, D12312, doi:10.1029/2005JD006744, 2006.

Redelsperger, J.-L., Thorncroft, C. D., Diedhiou, A., Lebel, T., Parker, D. J., and Polcher, J.: African monsoon multidisciplinary analysis: An international research project and field campaign, B. Am. Meteor. Soc., 87, 1739–1746, 2006.

Roca, R., Viollier, M., Picon, L., and Desbois, M.: A multi satellite analysis of deep convection and its moist environment over the Indian Ocean during the winter monsoon, J. Geophys. Res., 107, 8012, doi:10.1029/2000JD000040, 2002.

Rosenlof, K., Oltmans, S., Kley, D., Russell III, J. M., et al.: Stratospheric water vapour increases over the past half-century, Geophys. Res. Lett., 28(7), 1195–1198, 2001.

Scherer, M., Vömel, H., Fueglistaler, S., Oltmans, S. J., and Staehelin, J.: Trends and variability of midlatitude stratospheric water vapour deduced from the re-evaluated Boulder balloon series and HALOE, Atmos. Chem. Phys., 8, 1391–1402, doi:10.5194/acp-8-1391-2008, 2008.

Schiller, C., Grooß, J.-U., Konopka, P., Plöger, F., Silva dos Santos, F. H., and Spelten, N.: Hydration and dehydration at the tropical tropopause, Atmos. Chem. Phys., 9, 9647–9660, doi:10.5194/acp-9-9647-2009, 2009.

Schmetz, J., Tjemkes, S. A., Gube, M., and van de Berg, L.: Monitoring deep convection and convective overshooting with METEOSAT, Adv. Space Res., 19, 433–441, 1997.

Seidel, D. J., Ross, R. J., Angell, J. K., and Read, G. C.: Climatological characteristics of the tropical tropopause as revealed by radiosondes, J. Geophys. Res., 106, 7857–7878, 2001.

Solomon, S., Rosenlof, K. H., Portmann, R. W., Daniel, J. S., Davis, S. M., Sanford, T. J. and Plattner, G.-K. : Contributions of Stratospheric Water Vapor to Decadal Changes in the Rate of Global Warming, Science, 327, 5970, 1219–1223, doi:10.1126/science.1182488, 2010.

Stohl, A. and Seibert, P.: Accuracy of trajectories as determined from the conservation of meteorological tracers, Q. J. Roy. Meteor. Soc., 124, 1465–1484, 1998.

Zipser, E. J., Cecil, D. J., Liu, C., Nesbitt, S. W., and Yorthy, D. P.: Where are the most intense thunderstorms on Earth?, B. Am. Meteor. Soc, 87, 1058–1072, 2006.